의학박사 학위논문

Mechanism of TRPC4 activation by polycystin-1 and its regulation of Ca^{2+}-dependent signals in endothelium

폴리시스틴-1 에 의한 TRPC4 이온통로 활성화 기전 및 내피세포의 칼슘의존성 신호전달 조절

2017 년 02 월

서울대학교 대학원
의과학과 의과학 전공
곽 미 선

A thesis of the Degree of Doctor of Philosophy

폴리시스틴-1 에 의한 TRPC4 이온통로 활성화 기전 및 내피세포의 칼슘의존성 신호전달 조절

Mechanism of TRPC4 activation by polycystin-1 and its regulation of Ca^{2+}-dependent signals in endothelium

February 2017

The Department of Biomedical Sciences,
Seoul National University
College of Medicine
Misun Kwak

Mechanism of TRPC4 activation by polycystin-1 and its regulation of Ca^{2+}-dependent signals in endothelium

by
Misun Kwak

A thesis submitted to the Department of Physiology in partial fulfillment of the requirements for the Degree of Doctor of Philosophy in Medical Science at Seoul National University College of Medicine

January 2017

Approved by Thesis Committee:

Professor _____Chairman
Professor _____Vice chairman
Professor _____
Professor _____
Professor _____

ABSTRACT

Autosomal dominant polycystic kidney disease (ADPKD) is a common genetic disorder caused by polycystin-1 and polycystin-2 mutations. Hypertension and aneurysm are frequently associated with polycystic kidney disease, which is closely related to endothelial dysfunction. Polycystin-1 is an atypical G protein-coupled receptor that activates G protein by self-cleavage, induces intracellular signaling via activated G protein, and cell response by ion channel activation has been reported. TRPC4 is a calcium-permeable cation channel and is activated by a specific subtype of G protein ($G\alpha_i$). In this study, I hypothesized that polycystin-1 acts as a G protein-coupled receptor and activates G protein, resulting in TRPC4 activity. The C-terminus of polycystin-1 contains a G protein binding domain and selectively bound to $G\alpha_{i3}$ among the inhibitory G protein subtypes. The increase of TRPC4 activity by polycystin-1 was mediated by $G\alpha_{i3}$ and its mechanism was found to be the dissociation of the $G\alpha_{i3}$ from cleavage of PC1 C-terminus. Calcium influx through TRPC4 activated signal transducer and activator of transcription (STAT) and nuclear factor of activated T cells (NFAT) transcription factor to

regulate cell proliferation and death. In endothelial cells, endogenous expression and calcium influx of polycystin-1 and TRPC4 were observed. Inhibition of their expression or antagonist inhibited endothelial cell migration and weakened endothelial junctions. These results suggest that TRPC4 activity by polycystin-1 is important for endothelial cell monolayer formation and permeability through endothelial cells, and that TRPC4 is a target in the mechanism and treatment of aneurysms associated with ADPKD.

Keywords: ADPKD, PC1, GPCR, TRPC4, Ca^{2+}, STAT, NFAT, endothelial cells

Student number: 2013-23520

CONTENTS

LIST OF TABLES AND FIGURES

LIST OF ABBREVIATIONS

ADPKD, autosomal dominant polycystic kidney disease

aGPCRs, adhesion GPCRs

BAPTA, bis (2−aminophenoxy) ethane tetraacetic acid

CCh, carbachol (carbamylcholine)

Co−IP, co−immunoprecipitation

CPA, cyclopiazonic acid

CsA, cyclosporine A

CTF, C−terminal fragment

CTT, C−terminal tail

DMEM, Dulbecco's modified Eagle's medium

EGTA, Ethylene glycol−bis (β−aminoethyl ether) tetraacetic acid

FBS, fetal bovine serum

FRET, fluorescence resonance energy transfer

Gα_i, inhibitory Gα

Gα_iCA, constitutive active form of Gα_i protein

Gα_i DN, dominant negative form of Gα_i protein

GPCR, G protein−coupled receptor

GPS, G protein−coupled receptor proteolytic site

GSK3β, glycogen synthase kinase 3β

HEK 293, human embryonic kidney 293

HEPES, 10 N−[2−hydroxyethyl]piperazine−N' −[2−ethanesulfonic acid]

HUVEC, human umbilical vein endothelial cells

IB, immunoblot

JAK, Janus kinase

LDL-A, low-density lipoprotein-A domain

LRR, leucine-rich repeat

LRRCT, leucine-rich repeat C-terminus

LRRNT, leucine-rich repeat N-terminus

MDCK, Madin-Darby canine kidney cells

mIMCD-3, Mouse inner medullar collecting duct

NFAT, nuclear factor of activated T-cells

NTF, N-terminal fragment

PC1, polycystin-1

PC2, polycystin-2

PNGase F, peptide-N-Glycosidase F

REJ, receptor for egg jelly

SEM, standard error of the mean

SERCA, sarcoplasmic/endoplasmic reticulum Ca^{2+}-ATPase

SP, signal peptide

STAT, signal transducer and activator of transcription

TM, transmembrane

TRP, transient receptor potential channel

TRPC, classical type of TRP

TRPP, polycystic type of TRP

WSC, cell wall integrity and stress response component 1

WT, wild-type

INTRODUCTION

Autosomal dominant polycystic kidney disease (ADPKD) is one of the most common inherited diseases. It is characterized by the progressive expansion of multiple fluid-filled cysts in both kidneys, leading to end-stage renal failure (1). In ADPKD, the mutations of *PKD1* gene which encodes polycystin-1 (PC1) account for 85% of all cases. PC1 is involved in control of epithelial cell population growth (2, 3, 4, 5), migration (6, 7), differentiation (8) and apoptosis (9). In addition, PC1 is required for regulation of the cell cycle (10) and activation of cation permeable currents (11, 12, 13) by regulation of G-protein signaling (14, 15).

PC1 is a 4,302 amino acid glycoprotein (≥460 kDa) with 11 transmembrane domains, a large N-terminal extracellular region (3072 amino acid), and a short C-terminal cytoplasmic tail (~200 amino acid) (**Figure 1**) (16). A number of characteristic protein motifs are contained in the extracellular domain (**Table 1**). Leucine-rich repeats (LRRs) are responsible for interaction with the extracellular matrix and cell adhesion. The following domains are the cell wall integrity and

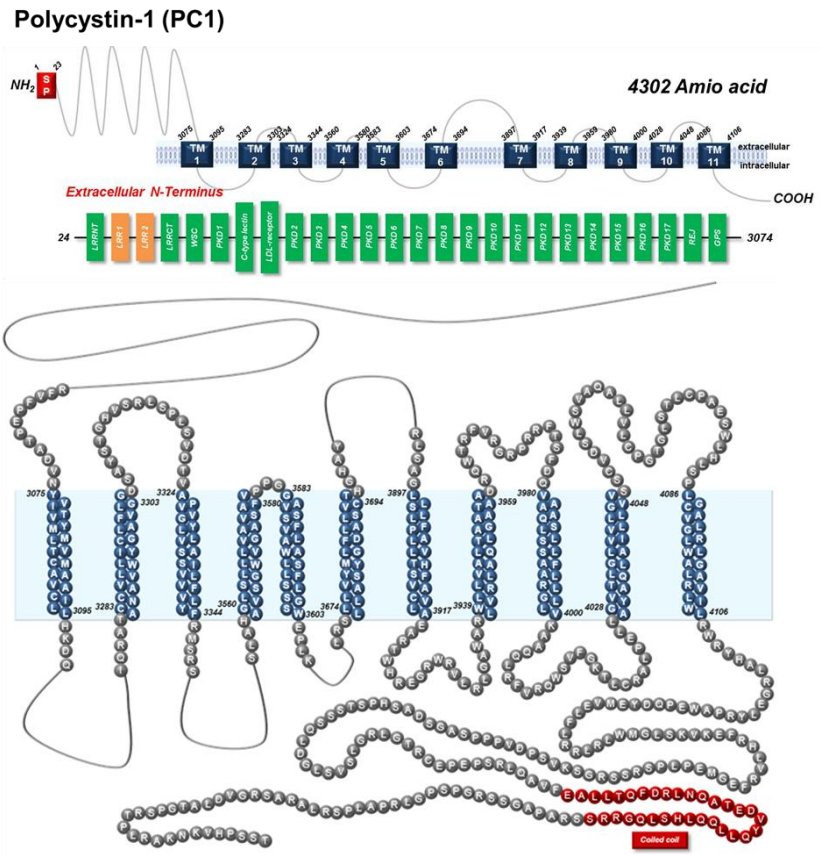

Figure 1. Domain structure of polycystin-1 (PC1).

SP, signal peptide; LRRNT, leucine-rich repeat N-terminus; LRRs, leucine-rich repeats; LRRCT, leucine-rich repeat C-terminus; WSC, cell wall integrity and stress response component 1; 17 PKD repeats, IgG-like domain; C-type lectin, lectin C type-3 domain; LDL-A, low-density lipoprotein-A domain; REJ, homology with sea urchin receptor for egg jelly; GPS, G-protein coupled receptor proteolytic site; TMs, transmembrane domains.

Table 1. Position of the PC1 domains based on human (GenBank accession number U24497.1).

Feature key	Position(s)	Length	Description
Domain	24-67	44	LRRNT
Repeat	68-91	24	LRR1
Repeat	92-113	22	LRR2
Domain	125-178	54	LRRCT
Domain	177-271	95	WSC
Domain	272-359	88	PKD1
Domain	415-531	117	C-type lectin
Domain	638-671	34	LDL-receptor class A; atypical
Domain	743-817	75	PKD2
Domain	855 - 928	74	PKD3
Domain	935-1020	86	PKD4
Domain	1023-1129	107	PKD5
Domain	1127-1215	89	PKD6
Domain	1213-1298	86	PKD7
Domain	1294-1383	90	PKD8
Domain	1382-1469	88	PKD9
Domain	1468-1551	84	PKD10
Domain	1550-1635	86	PKD11
Domain	1634-1721	88	PKD12
Domain	1719-1805	87	PKD13
Domain	1807-1890	84	PKD14
Domain	1889-1974	86	PKD15
Domain	1977-2057	81	PKD16
Domain	2060-2148	89	PKD17
Domain	2146-2833	688	REJ
Domain	3012-3061	50	GPS
Domain	3118-3233	116	PLAT

stress response component (WSC) domain, thought to interaction with carbohydrates, and a lectin C-type motif, involved in biological processes such as cellular signaling and exocytosis. PC1 has 17 PKD repeats that share sequence similarity with immuno-globulin-like and fibronectin type-3 domains. Such repeats are stabilized by formation of a stable intermediate state which consistent with a role for PC1 in mechanical coupling between cells. A receptor for the egg jelly (REJ) domain is implicated as a novel effector site for normal function of PC1. A GPS domain, the potential proteolytic cleavage site, is situated between the REJ and the first transmembrane of PC1 (17). The C-terminal cytosolic domain includes a coiled-coil domain that has been implicated in interactions with the C-terminus of TRPP2 (PC2) as well as a variety of other proteins involved in cellular signaling (18, 19). Also, the C-terminal of PC1 contains a G protein activation site, suggesting a potential role in the regulation of G protein intracellular signaling.

PC1 is considered as an atypical G-protein coupled receptor (GPCR) based on binding Gα proteins and regulating ions influx through channels via release G$\beta\gamma$ subunits (15). When

expressed alone, PC1 can activate a G-protein signaling pathway by direct binding and activation of heterotrimeric $G\alpha_{i/o}$ proteins and consequently modulates voltage-gated Ca^{2+} channels and GIRK K^+ channels via the release of $G\beta\gamma$ subunits. Abnormal G-protein mediated signaling may contribute to cyst formation by modulating cellular proliferation, transepithelial fluid secretion, and differentiation mediated by adenylate cyclase and mitogen-activated protein kinase pathways. However, whether PC1 can activate G proteins in a physiologically relevant cell type is currently unknown.

A fundamental property of PC1 is post-translational modification by proteolytic cleavage at the GPS domain (17). PC1 undergoes cleavage at the HL↓T ^{3049} tripeptide sequence within the GPS domain. PC1 is also cleaved at specific sites in C-terminal domains (**Figure 2**). The products of these cleavages can be induced by many factors (**Figure 3**). Cleavage of PC1 at the GPS domain promotes formation of various C-terminal fragments or tails (CTFs or CTTs) which modulate diverse signaling pathway via translocation to the nucleus (20). Thus, missense mutations in the GPS domain disrupt cleavage of PC1 and prevent a number of intracellular signaling pathways,

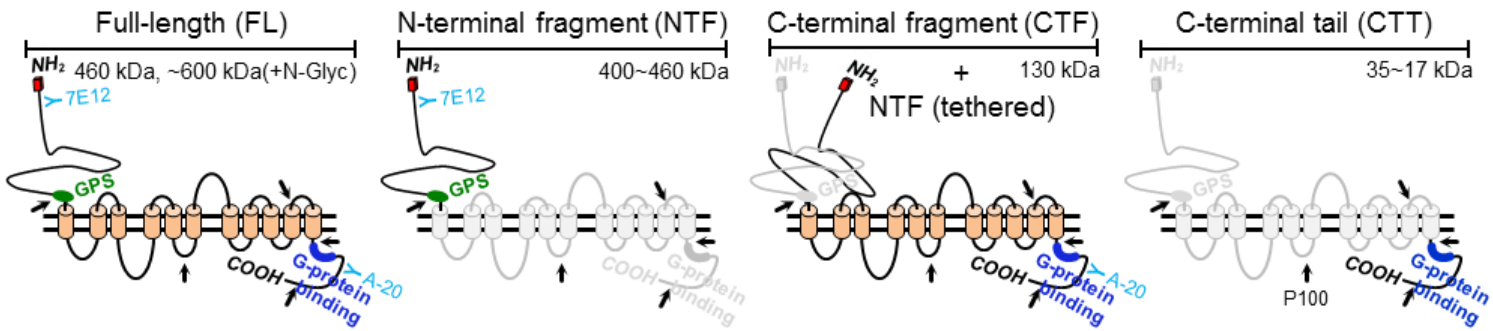

Figure 2. Schematic representation of PC1 isoforms.

PC1 is cleaved at the GPS, resulting in N−terminal fragment (NTF, 400~600 kDa) and C−terminal fragment (CTF, 130 kDa). The cleaved NTF can either be released or remain tethered to the CTF. C−terminal tail (CTT) is cleaved at a minimum of two different sites, generating two products (28 to 34 kDa and ~17 kDa). P100, a 100 kDa fragment, is derived from proteolytic cleavage within the third intracellular loop.

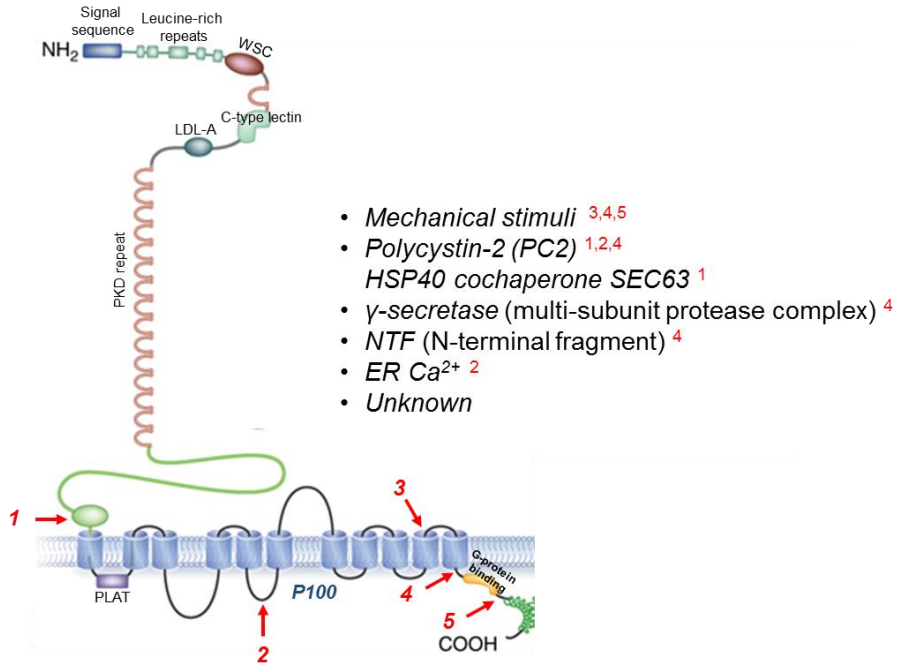

Figure 3. Cleavage-inducible factors of PC1.

PC1 is a large protein that is predicted to possess a large N-terminal extracellular domain (NH_2), 11 transmembrane segments (blue), and a short cytoplasmic C-terminal tail (COOH). The various factors induce the cleavage of PC1 and exist such as mechanical stimuli, polycystin-2, SEC63, γ-secretase, N-terminal fragment (NTF), and ER Ca^{2+}. Sites of cleavage by each inducible factor were indicated by red arrow.

including JAK/STAT (21), Wnt (22), mTOR (23), NFAT (24) and Ca^{2+} homeostasis (5, 25).

Signal transducer and activator of transcription (STAT) protein family are intracellular transcription factors that mediate many aspects of cellular immunity, proliferation, apoptosis and differentiation. STAT proteins are tyrosine phosphorylated by members of the Janus kinase (JAK) family, tyrosine kinase growth factor receptors, nonreceptor tyrosine kinases, and seven transmembrane pass receptors (26). The JAK/STAT signaling pathway has been described to mediate polycystin signaling (10, 27). The cleaved PC1 tail interacts with the transcription factors STAT6 and P100. It enhances activity and translocation of STAT6 between cilia and the nucleus, depending on luminal fluid flow stimulation. Overexpression of full-length PC1 leads to activation of STAT1 and STAT3. The mechanism of STATs up-regulation and activation in ADPKD remains unclear and requires further study.

The cellular target for Ca^{2+} increases is a ubiquitous serine-threonine phosphatase, calcineurin, and its intracellular substrate nuclear factor of activated T-cells (NFAT). The inactive hyperphosphorylated form of NFAT is localized in the

cytosol. NFAT is dephosphorylated upon calcineurin activation following increased Ca^{2+} influx. NFAT translocation into the nucleus influences the regulation of target genes, often at composite NFAT/AP-1 elements (28). Termination of NFAT signaling occurs through rephosphorylation of NFAT by glycogen synthase kinase 3β (GSK3β) and relocation back to the cytoplasm. The immunosuppressive drugs, cyclosporine A (CsA) and FK506, inhibit calcineurin and nuclear translocation of NFAT. Activation of calcineurin/NFAT signaling has been shown to control cell differentiation, apoptosis and cellular adaptation in a wide variety of cell types and tissues, and to regulate the non-canonical Wnt/Ca^{2+} pathway during embryonic development. Regulation of intracellular Ca^{2+} has been previously associated with the function of PC1 (24). Thus, it speculates that PC1 might trigger the calcineurin/NFAT signaling pathway ultimately leading to modulation of NFAT target genes expression.

Transient receptor potential (TRP) channels consist of a family of seven cationic channels, which are divided by some structural similarity. TRPs can form functional homo- or hetero-tetrameric channels with intra-subgroup even with

inter-subfamilies (29). The polycystic type of TRP (TRPP) channel is associated with polycystic kidney disease which results from abnormal Ca^{2+} homeostasis and signaling (30). Newby LJ et al. (31) suggested that the PC1/PC2 as receptor-ion channel complex plays a critical role in renal physiology. The classical type of TRP (TRPC) is receptor-operated channel (via G protein-coupled) which is primarily activated in response to PLC activation (32) or inhibitory $G\alpha$ ($G\alpha_i$) interaction (33). I expected that PC1 can activate TRPC4 channel depending on $G\alpha_i$ through dissociation of heterotrimeric $G\alpha_{i/o}\beta\gamma$ protein.

Vascular endothelial cell Ca^{2+} entry through TRPC4 leads to vascular smooth muscle relaxation and the endothelial hyper-permeability via disruption of cell junction complexes or cytoskeletal reorganization (34). Cerebral aneurysms are more common in ADPKD patients who are caused by loss of function and missense mutations in PC1 encoding *PKD1* gene (35, 36, 37). Accordingly, the function of TRPC4 with PC1 is essential for Ca^{2+} regulation in endothelium that remains unknown.

My results, obtained on HEK 293 cells overexpressed with recombinant TRPC4 and PC1, are analyzed by ion channel

activity using electrophysiological technique and by Ca^{2+}-dependent signaling using molecular biologic methods. In this study, I identified that the stimulation of $G\alpha_{i3}$ by PC1 cleavage activates TRPC4β channel. Following this result, influx of cytosolic Ca^{2+} triggers the activation of STATs and NFAT. Taken together, these finding suggest that $G\alpha_{i3}$ -mediated TRPC4 activation by polycystin-1 may contribute to endothelial function.

MATERIALS AND METHODS

1. Cell culture and transfection

Human embryonic kidney (HEK)-293 cells (American Type Culture Collection, USA) were maintained in Dulbecco's modified Eagle's medium (Hyclone, USA) supplemented with 10 % fetal bovine serum (FBS), 100 U/ml penicillin, and 100 ㎍/ml streptomycine according to the supplier's recommendations. Mouse inner medullar collecting duct (mIMCD-3) and Madin-Darby canine kidney cells (MDCK) were cultured in Dulbecco's modified Eagle's medium/F12 medium supplemented with 10 % FBS. Human umbilical vein endothelial cells (HUVECs) were cultured in M199 medium containing 10 % FBS, sodium heparin (100 units/㎖, Sigma), endothelial cell growth supplement (50 ㎍/㎖, BD), and antibiotics. For transient transfection, cells were seeded in 6- or 12-well plates. On the next day, 0.5-2 ㎍/well of TRPC4β and PKD1 cDNA was transfected into cells using the transfection reagent FuGENE 6 (Roche Molecular Biochemicals, USA) for electrophysiological experiments or Lipofectamine 2000 (Invitrogen, USA) for molecular biology tool according to

the manufacturer's protocol. All experiments were performed after 20-30 h from transfection.

2. Plasmids

Plasmid human PKD1 (FL) in pGFP-N1 and human PKD1 (FL)-Flag in pCI-neo were kindly provided by Eric Honoré and Gregory Germino, respectively. HA-human PKD1 (CTF)-Flag in pCI and EGFP-human PKD1 (FL) in pCI were kindly provided by Feng Qian (Johns Hopkins University). Human PKD1 (FL) was subcloned into the pECFP-N1 and pEYFP-N1 vectors.

3. Western blot analysis

Cells were plated in 6-well dishes. Lysates were prepared in lysis buffer (0.5 % Triton X-100, 150 mM NaCl, 50 mM HEPES, 2 mM MgCl2, 2 mM EDTA, pH 7.4) by passage 10-15 times through a 26-gauge needle after sonication. Lysates were centrifuged at 13,000 x g for 10 min at 4 ℃, and the protein concentration in the supernatants was determined. The proteins extracted in sample buffer were loaded onto 5, 8, or 10 % Tris-glycine sodium dodecyl sulphate polyacrylamide gel

electrophoresis (SDS-PAGE) gels. The proteins were transferred onto a PVDF membrane. The table below provides information of antibodies.

Table 2. Experimental conditions used in Western blot analysis.

Target protein	Company	Cat. No.	Titer
PC1	Santa cruz	sc-130554	1:1000
PC1	Santa cruz	sc-10371	1:1000
GFP	Life technologies	A11122	1:5000
Gα_o	Santa cruz	sc-13532	1:1000
Gα_{i1}	Santa cruz	sc-56536	1:1000
Gα_{i2}	Santa cruz	sc-13534	1:1000
Gα_{i3}	Santa cruz	sc-262	1:1000
Gα_q	Santa cruz	sc-136181	1:1000
Gα_s	Santa cruz	sc-823	1:1000
Gα_{12}	Santa cruz	sc-409	1:1000
STAT1	Cell signaling	#9172	1:1000
pSTAT1^{Y701}	Cell signaling	#9167	1:1000
STAT3	Cell signaling	#9132	1:1000
pSTAT3^{Y705}	Cell signaling	#4113	1:1000
NFATc1	Santa cruz	sc-7294	1:1000
NFATc2	Santa cruz	sc-7296	1:1000
NFATc3	Santa cruz	sc-8321	1:1000
NFATc4	Santa cruz	sc-13036	1:1000
TRPC4	Neuromab	73-119	1:200
β-tubulin	Sigma	T-4026	1:5000
β-actin	GeneTex	GTX109639	1:5000

4. Co-immunoprecipitation and surface biotinylation

In the co-IP experiments for the detection of PC1-Gα subtypes, 500 ㎕ of cell lysates (500-1000 ㎍) were incubated with 1 ㎍ of anti-PC1 (A-20) or anti-Gα antibodies and 30 ㎕ of protein G-agarose beads at 4 ℃ overnight with gentle rotation. Next, the beads were washed three times with wash buffer (0.1 % Triton X-100), and the precipitates were eluted with 30 ㎕ of 2 x Laemmli buffer and subjected to Western blot analysis.

For surface biotinylation, PBS-washed cells were incubated in 0.5 ㎎/㎖ sulfo-NHS-LC-biotin (Pierce, USA) in PBS for 30 min on ice. Afterwards, the biotin was quenched by the addition of 100 mM glycine in PBS. The cells were then processed as described above to make cell extract. Forty microliters of 1:1 slurry of immobilized avidin beads (Pierce, USA) were added to 300 ㎕ of cell lysates (500 ㎍ protein). After incubation for 1h at room temperature, beads were washed three times with 0.5 % Triton X-100 in PBS, and proteins were extracted in sample buffer. Collected proteins were then analyzed by Western blot.

5. Deglycosylation

Transiently transfected HEK 293 cells were lysed and treated with PNGase F (New England Biolabs, MA) according to manufacturer's instruction, followed by Western blot analysis.

6. Electrophysiology

Transfected cells were trypsinized and transferred into a recording chamber equipped to treat with a number of solutions. Whole cell currents were recorded using an Axopatch 200B amplifier (Axon Instruments, USA), Digidata 1440A Interface (Axon Instuments), and analyzed using a personal computer equipped with pClamp 10.2 software (Axon Instruments) and Origin software (Microcal origin v.8.0, U.S.A.). Patch pipettes were constructed from borosilicate glass and had resistances of 2-4 MΩ when filled with standard intracellular solutions. For whole cell experiments, I used an external bath medium (normal Tyrode solution) of the following composition : 135 mM NaCl, 5 mM KCl, 2 mM $CaCl_2$, 1 mM $MgCl_2$, 10 mM glucose, and 10 N-[2-hydroxyethyl]piperazine-N'-[2-ethanesulfonic acid] (HEPES) with pH adjusted to 7.4 using NaOH. Cs^+-rich external solution was made by replacing NaCl and KCl with

equimolar CsCl. The standard pipette solution contained 140 mM CsCl, 10 mM HEPES, 0.2 mM Tris-GTP, 0.5 mM EGTA, and 3 mM Mg-ATP with pH adjusted to 7.3 using CsOH. Voltage ramp pulses were applied from +100 to -100 mV for 500 ms at -60 mV holding potential. All current traces are drawn from the selected at -60 or +80 mV of the ramp pulses.

7. Fluorescence resonance energy transfer measurement

Three fluorescence resonance energy transfer (FRET) images (cube setting for CFP, YFP and Raw FRET) were obtained from a pE-1 Main Unit to 3 FRET cubes (excitation, dichroic mirror, filter) via a fixed collimator. The excitation LED and filter were sequentially rotated, and the rotation period for each of filter cubes was ~0.5 s. All of the images were obtained within 1.5 s. Each of the images was captured on a cooled 10 MHz (14 bit) CCD camera (ANDOR technology, USA) with an exposure time of 100 ms with 2x2 binning (645x519 pixels). Using an IX70, Olympus microscope equipped with a 60 x oil objective, the three-cube FRET efficiency was analyzed using MetaMorph 7.6 software (Molecular Devices, USA). Data obtained from

each individual cell were used to calculate the ratios and reflective of the energy transferred.

8. Intracellular Ca^{2+} measurement with Fura-2

The ratiometric measurement of $[Ca^{2+}]_i$ was performed using Fura-2-AM (molecular probe, USA). The cells were grown in 24-well dishes and loaded with 5 μM of Fura-2-AM for 30 min at 37 ℃. The Fura-2 fluorescence was measured at a 510 nm emission with a 340/380 nm dual excitation using a DG-4 illuminator. The experiments were performed in a normal solution containing 145 mM NaCl, 3.6 mM KCl, 10 mM HEPES, 1.3 mM $CaCl_2$, 1 mM $MgCl_2$, and 5 mM glucose with pH adjusted to 7.4 using NaOH.

9. Wound-healing assay

HUVEC transfected with PC1 siRNA or STATs siRNA were seeded in 6 well culture plates and incubated with ML204, a selective TRPC4 channel inhibitor. Cells were grown as high-density monolayers, scratched with a 200 $\mu\ell$ pipette tip, and after three washes to remove detached cells, allowed to migrate for the indicated time. Migration was recorded using a Nikon

ECLIPSE TS100 microscope equipped with Lumenera's INFINITY1-3 digital camera. The area covered by the monolayer was measured using ImageJ (National Institutes of Health). All migration assays are representative of at least three independent experiments.

10. Luciferase assay

HEK 293 cells were transfected as described above. 24 h after transfection, cells were lysed and analyzed for luciferase activity by a Dual-Luciferase Reporter Assay System (Promega). The assays were repeated at least three times, and the activity of firefly luciferase (pGL4) was normalized to that of the internal control.

11. Statistical analyses

Results are presented as the mean ± standard error of the mean (SEM). The results were compared using Student's t test between two groups or using ANOVA followed by post hoc test among three or more groups. $p<0.05$ was considered to be statistically significant. The number of cell electrical recording is given by n in the bar graph.

RESULTS

Identification of polycystin-1 (PC1)

The polycystin-1 (PC1) undergoes several proteolytic cleavages, including an autocatalytic cleavage at the G protein-coupled receptor proteolytic site (GPS). The cleaved PC1 form consisting of the N-terminal fragment (NTF) associated with the C-terminal fragment (CTF) and at least three other cleavages liberate portions of the cytoplasmic C-terminal tail (CTT) of PC1 (38). PC1 is a large plasma membrane glycoprotein and includes many N-linked glycosylation sites predicted by the 'NetNGlyc' (**Figure 4A and Figure 5**). To detect PC1 *in vitro*, I performed immunoblot (IB) analysis with an anti-PC1 antibody (7E12) from lysates of flag-tagged human *PKD1* expression in HEK293 cells. As shown in **Figure 4B**, two bands at ≥460 kDa were observed. To clarify what that means, I confirmed shift of two bands upon peptide-N-Glycosidase F (PNGase F) treatment. If the upper band was glycosylated full-length PC1 and the lower band was full-length PC1 (PC1 (FL)), one band would be observed after treatment with PNGase F. Or if each of two bands was glycosylated full-length PC1 and N-terminal fragment,

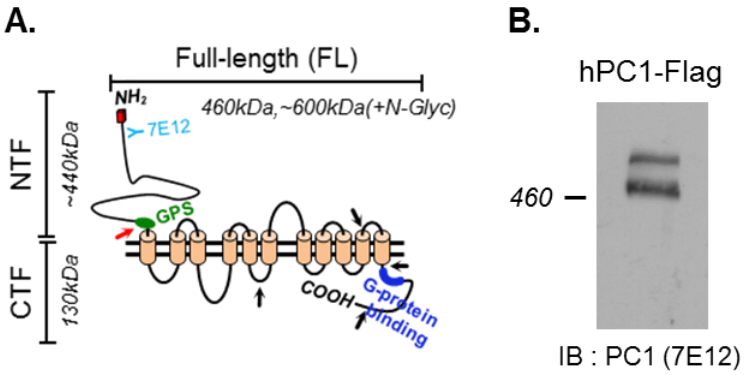

Figure 4. Schematic diagram of PC1 structure and identification of PC1 products. (A) Schematic structure of human PC1. FL, full-length; NTF, N-terminal fragment; CTF, C-terminal fragment; GPS, G protein-coupled receptor proteolytic site. PC1 cleavage occurs at GPS motif, resulting in NTF and CTF fragments. At least three proteolytic cleavages take place in or near its C-terminal tail that result in the release of protein fragments. The possible cleavage sites are shown by arrows. A blue color code indicates epitope recognized by anti-PC1 antibody (7E12). (B) Flag-tagged full-length human PC1 was expressed in HEK 293 cells and analyzed by Western blotting using antibodies as indicated.

Figure 5. Potential *N*-glycosylation sites of PC1.

Predicted N-glycosylation sites are colored in red. 11 transmembrane (TM) segments are shown by yellow boxes.

two forms of glycosylated PC1 with PNGase F treatment would be migrated. As shown in Figure 6, treatment with PNGase F reduced the size of the glycosylated upper and lower bands, indicating that an antibody against PC1 N-terminus can detect full-length and N-terminal fragment of PC1.

To determine PC1 expression pattern using variously tagged (GFP, Flag, and HA) constructs at the each terminus of the PC1 (Figure 7A), I performed Western blot analysis with several detectable antibodies. Additionally, other hPC1(FL) constructs which were cloned into pECFP-N1 and pEYFP-N1 were made and used for imaging experiment. As mentioned above, various forms of PC1 were observed through antibodies (Table 3). Figure 4B showed that all constructs indicated FL and NTF of glycosylated PC1 at 520 and 440 kDa, respectively. FL, CTF and CTF-GFP, a cleavage product of hPKD1-GFP, was detected by an anti-PC1 antibody (A-20) (Figure 7C). In contrast, predicted molecular weight (157 kDa) of CTF (130 kDa) containing GFP (27 kDa) was not observed in cloned constructs (hPC1-ECFP and hPC1-EYFP). The distribution among them was also different.

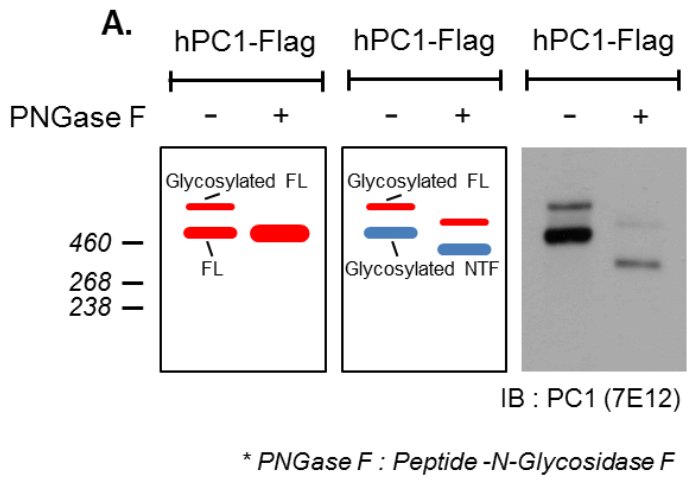

Figure 6. *N*-glycosylation analysis of PC1.

Western blot analysis, using an anti-PC1 antibody (7E12), of lysates from HEK 293 cells transiently transfected with expression construct encoding PC1 (FL). Two bands of PC1 is shifted to a lower molecular mass in the presence of PNGase F. Bands indicate glycosylated full-length of PC1 (upper band) and glycosylated N-terminal fragment of PC1 (lower band), respectively. Schematic diagram (left panel) provides an identification guide.

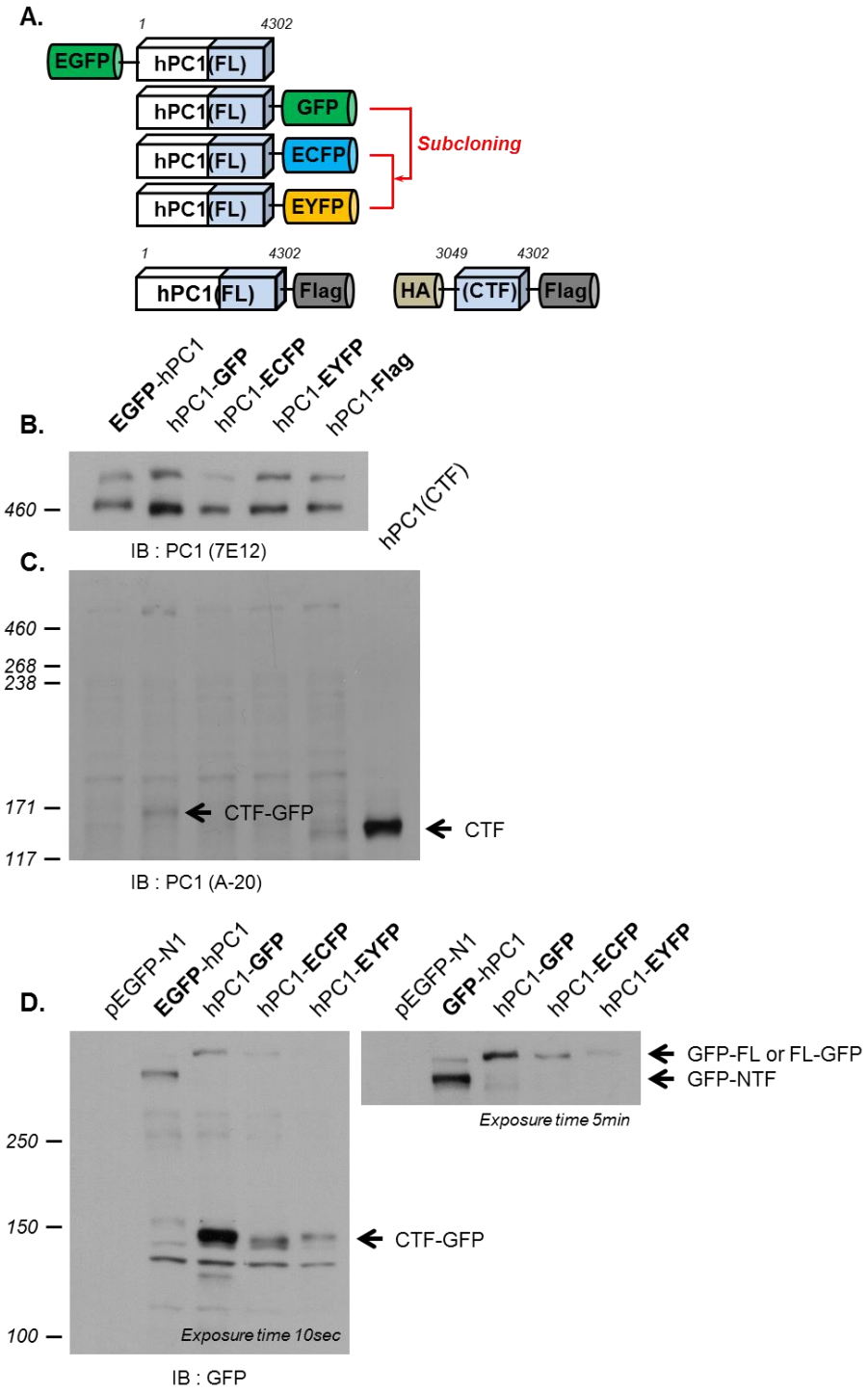
A.
1
4302
EGFP
hPC1(FL)
hPC1(FL)
GFP
hPC1(FL)
ECFP
hPC1(FL)
EYFP
Subcloning
1
4302
3049
4302
hPC1(FL)
Flag
HA
(CTF)
Flag
B.
EGFP-hPC1
hPC1-GFP
hPC1-ECFP
hPC1-EYFP
hPC1-Flag
460
hPC1(CTF)
IB : PC1 (7E12)
C.
460
268
238
171
117
CTF-GFP
CTF
IB : PC1 (A-20)
D.
pEGFP-N1
EGFP-hPC1
hPC1-GFP
hPC1-ECFP
hPC1-EYFP
pEGFP-N1
GFP-hPC1
hPC1-GFP
hPC1-ECFP
hPC1-EYFP
GFP-FL or FL-GFP
GFP-NTF
Exposure time 5min
250
150
100
CTF-GFP
Exposure time 10sec
IB : GFP

Figure 7. Validation of PC1 constructs.

(A) Schematic representation of human PC1 constructs. C-terminal fragment (CTF) of PC1 is indicated by blue square. (B) HEK 293 cells were transfected with expression constructs encoding the X-fusion PC1 (FL), either tagged at the C- or N-terminal. The proteins were detected with an anti-PC1 antibody (7E12). FL and NTF forms of PC1 were observed in all lysates from transiently transfected HEK 293 cells expressing hPC1. (C) HEK 293 cells were transfected with indicated plasmids. The cleaved CTF forms were detected by IB with anti-PC1 antibody (A-20) (black arrow). (D) HEK 293 cells were transiently transfected with (pEGFP-N1, lane 1), EGFP-tagged hPC1 (lane 2), hPC1-GFP (lane 3), hPC1-ECFP (lane 4), or hPC1-EYFP (lane 5). X-tagged proteins were immunoblotted with anti-GFP (black arrow). Two blot exposures are shown.

Table 3. Recognized cleavage form of PC1 by antibodies.

	The molecular size of Polycystin-1(PC1), kDa				
Isoforms of PC1	FL (520kDa)	NTF (440 kDa)	CTF (130 kDa)	P100 (100 kDa)	CTT (35, 17 kDa)
	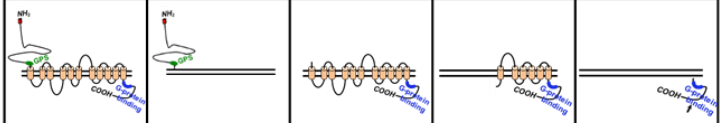				
7E12	**520**	**440**			
A-20	**520**		**130**	100	35
GFP (N-term. tagging)	547	467			
GFP (C-term. tagging)	**547**		**157**	127	62, 44
Flag (C-term. tagging)	520		130	100	35, 17

PC1 was observed in the nucleus as well as the cytosol and the plasma membrane (Figure 8A). I still did not find any differences between an original construct and cloned constructs despite the comparative analysis through sequence alignment. However, I supposed that such differences might be observed, because a part of PC1 CTT including an epitope recognized by anti-PC1 antibody (A-20) was lost by an unknown factor. As shown in Figure 5B, uncharacterized CTT form of PC1, protein with a molecular weight of about 20-27 kDa, was observed in over-expression of cloned constructs. Interestingly, various forms of PC1 recognizable by anti-GFP were detected in all constructs including cloned constructs (Figure 7D). Consequently, although PC1 has various forms of cleavage, cleavage-inducible factors are still unclear. Also, I suggest that unknown cleavage forms can exist.

Identification of endogenous polycystin-1 in various cell lines

At the tissue level, PC1 expression was observed in specific cell types in tissues with known manifestations of autosomal dominant polycystic kidney disease (ADPKD) (Figure 9). Expression was frequently seen in kidney, but also in gastro-

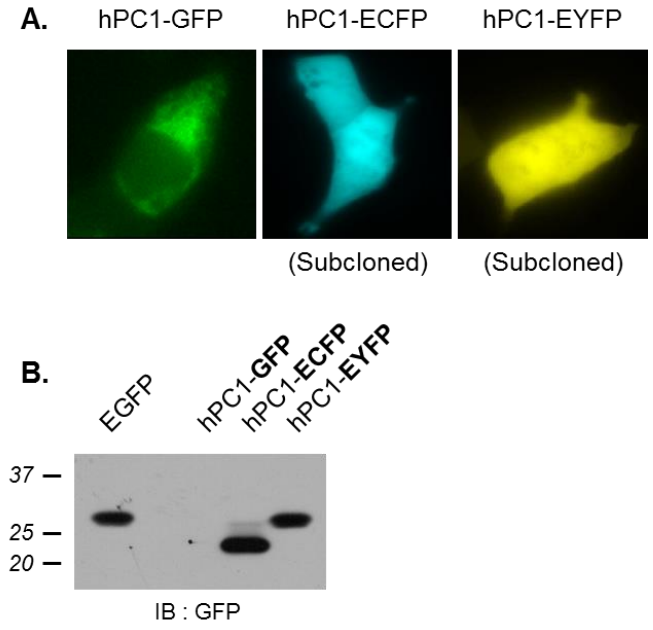

Figure 8. Identification of sub-cloned PC1 constructs.

(A) Fluorescence microscopic images of HEK 293 cells transfected with hPC1 (FL)-GFP (green), hPC1 (FL)-ECFP (cyan), and hPC1 (FL)-EYFP (yellow). (B) HEK 293 cells were transfected with sub-cloned PC1 constructs, respectively. Cell lysates were used for Western blot analysis with anti-GFP.

Organ		Protein (score)	RNA (FPKM)
Brain	Cerebral cortex		8.7
	Hippocampus		-
	Lateral ventricle		-
	Cerebellum		-
Endocrine tissues	Thyroid gland		1.7
	Parathyroid gland		-
	Adrenal gland		7.3
Bone marrow & immune system	Appendix		3.6
	Bone marrow		2.6
	Lymph node		3.2
	Tonsil		1
	Spleen		5.8
Muscle tissues	Heart muscle		7.1
	Skeletal muscle		8.1
	Smooth muscle		4.9
Lung	Nasopharynx		-
	Bronchus		-
	Lung		6.1
Liver & gallbladder	Liver		0.6
	Gallbladder		4.2
Pancreas	Pancreas		1.4
Skin	Skin		10
Adipose & soft tissue	Adipose		5.8
	Soft tissue		-
Gastrointestinal tract	Oral mucosa		-
	Salivary gland		4
	Esophagus		4.8
	Stomach		3.8
	Duodenum		2.6
	Small intestine		3.9
	Colon		3.7
	Rectum		1.1
Kidney & urinary bladder	Kidney		2.7
	Urinary bladder		3.5
Male tissues	Testis		6.6
	Epididymis		-
	Prostate		9.3
	Seminal vesicle		-
Female tissues	Breast		-
	Vagina		-
	Cervix, Uterine		-
	Endometrium		8.5
	Fallopian tube		6.4
	Ovary		9.2
	Placenta		4

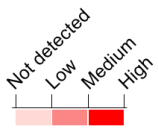

Figure 9. RNA and Protein expressions of PC1 in organs.

intestinal tract (stomach, duodenum, and small intestine). In addition, expression was observed in brain and more weakly in muscle tissues despite high RNA levels. The correlation between expression levels of RNA and protein was not shown.

Several studies report that the level of PC1 expression is critical for normal function including proper tubular differentiation and maturation (39). PC1 is predominantly expressed in ductal epithelial cells. Two immortalized renal epithelial cell lines, Madin-Darby canine kidney cells (MDCK) and mouse inner medullar collecting duct (mIMCD-3), have been widely used to study tubular kidney epithelial morphogenesis *in vitro*. To confirm expression of PC1 in two renal epithelial cell lines, I performed immunoblot with anti-PC1 antibody (7E12). Figure 10 showed that the predicted size of PC1 (FL) which was not an accurate estimate of the size of protein in lysates from each of the cell lines was observed. Thus, PC1 was indeed expressed in MDCK cells and mIMCD-3, but the level of expression was relatively low. Subsequently, I confirmed PC1 expression in MDCK with stable expression of the full-length human PC1 (MDCK PKD1-19). However, I did not observe a notable difference between the two MDCK

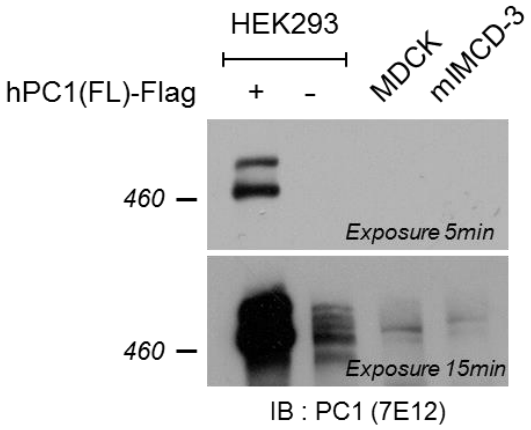

Figure 10. Expression of PC1 in MDCK cell and mIMCD-3.

HEK 293 cells with or without transient transfection of hPC1 (FL)-flag were immunoblotted with an anti-PC1 antibody (7E12). Endogenous PC1 in HEK 293, MDCK, and mIMCD-3 cells was immunoblotted by 7E12. Stronger endogenous PC1 expression can be seen in HEK 293 cells than in MDCK or mIMCD-3 cells.

cell lines (**Figure 11A**). Since sodium butyrate had been previously shown to enhance expression of recombinant proteins in mammalian cells, I confirmed this property in MDCK cell lines. The cell lines were treated with 20 mM sodium butyrate overnight and then reconfirmed expression of PC1. I was unable to observe the increase in PC1 expression after treatment by sodium butyrate. The result was presented in **Figure 11B**.

ADPKD is also characterized by cardiovascular, cerebrovascular, and connective tissue abnormalities. And abnormal endothelial cell function may contribute to the development of vascular abnormalities such as hypertension and cerebral aneurysms (40). I confirmed expression of PC1 in human umbilical vein endothelial cells (HUVEC) using anti-PC1 (7E12) and anti-PC1 (A-20) antibodies. As shown in **Figure 12A** and **Figure 12B**, PC1 existed in endothelial cells. These results show that expression of PC1 appears widespread, consistent with the systemic nature of the disease.

Cleavage of PC1

PC1 undergoes several cleavages. An autocatalytic event

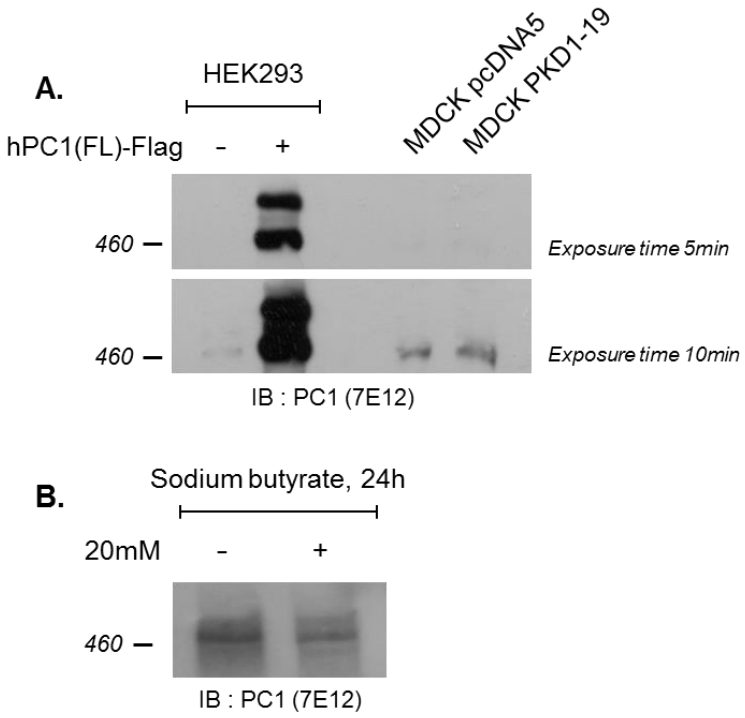

Figure 11. Expression of PC1 in MDCK cell lines.

(A) HEK 293 cells with or without transient transfection of hPC1(FL)-flag were immunoblotted with an anti-PC1 antibody (7E12). Endogenous PC1 in HEK 293 and MDCK cells, as well as overexpressed PC1 from the inducible stable cell line MDCK PKD1-19, was detected by anti-PC1 antibody (7E12). (B) Stable cell line (MDCK PKD1-19) was treated with 20 mM sodium butyrate overnight and then assayed for PC1 expression. Expression of PC1 was not altered in the presence or absence of 20 mM sodium butyrate.

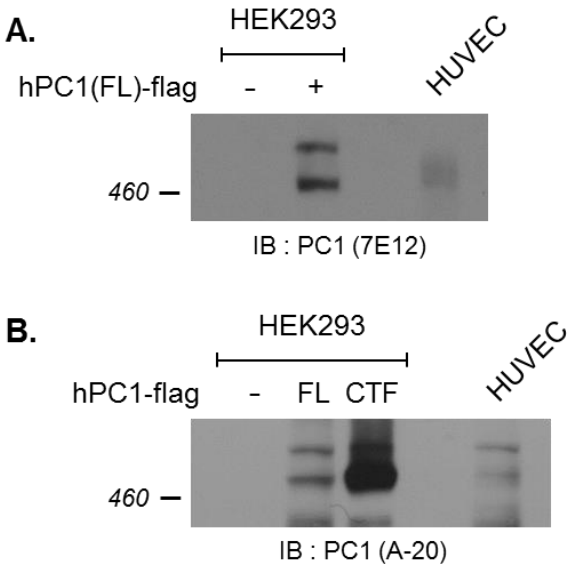

Figure 12. Expression of PC1 in HUVEC.

(A) HEK 293 cells with or without transient transfection of hPC1(FL)-flag were immunoblotted with an anti-PC1 antibody (7E12). Endogenous PC1 in HEK 293 cells and HUVEC was detected by anti-PC1 antibody (7E12). (B) HEK 293 cells with or without transient transfection of hPC1(FL)-flag and HA-hPC1(CTF)-flag were immunoblotted with an anti-PC1 antibody (A-20). Cleavage of endogenous PC1 in HUVEC was detected.

releases the N-terminal extracellular domain which remains non-covalently attached to the transmembrane domains (41). The CTT of PC1 is cleaved and translocated to the nucleus (42). And the products of these cleavages perform important physiological functions. Nevertheless, it is still not clear that how and where PC1 is cleaved. According to previously reported data, there are cleavage-inducible factors such as mechanical stimuli (42), polycystin-2 (PC2) (43), γ-secretase (44), and so on. Firstly, I confirmed effect of cleavage by fetal bovine serum (FBS) in culture media because cleavage of PC1 was detected in HEK293 cells transfected with a hPC1 (FL) without any treatment. Cleavage patterns of endogenous PC1 did not show differences in a dose dependent manner. Cleavage of PC1 was observed for all conditions, even if the amount of expressed protein was different (**Figure 13A**). As shown in **Figure 13B**, I could also obtain the same result in lysates from HEK293 cells expressing hPC1 (FL)-flag. These results suggest that cleavage of PC1 can appear by overexpression itself, but not FBS. Next, to determine whether cleavage of PC1 is influenced by Ca^{2+}, I transiently transfected with hPC1 (FL)-flag and incubated in the presence or

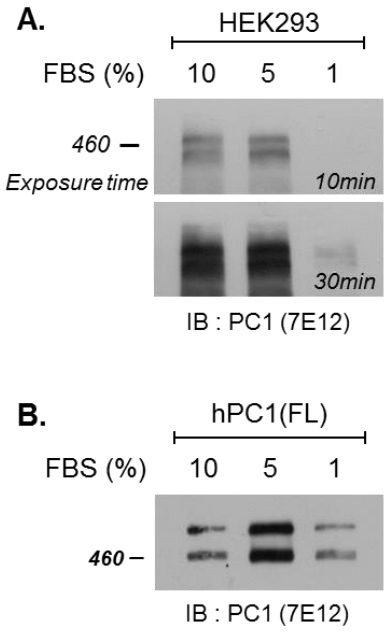

Figure 13. Cleavage of PC1 in a FBS-dependent manner.

(A) Fetal bovine serum (FBS) was treated with the indicated dose, and endogenous PC1 was immunoblotted using anti-PC1 antibody (7E12). Compared to normal condition (DMEM medium containing 10 % FBS), the 5 % FBS-treated HEK 293 cells did not find a significant difference. Although bottom blot was visualized by exposure for 10 minutes, 1 % FBS-treated HEK 293 cells was not detectable by immunoblotting. (B) FBS was treated with the indicated dose in HEK 293 cells with transient transfection of hPC1(FL)-flag. Cleavage of PC1 did not show any significant difference among the three conditions.

absence of reagents that regulate the levels of cytosolic Ca^{2+}. Extracellular Ca^{2+} was removed by Ca^{2+}-free media exchange. Ethylene glycol-bis (β-aminoethyl ether) tetraacetic acid (EGTA) and bis (2-aminophenoxy) ethane tetraacetic acid (BAPTA) was used to control the level of both intracellular and extracellular Ca^{2+}. Also, I confirmed a correlation between cleavage and depletion of ER Ca^{2+} using thapsigargin (TG) and cyclopiazonic acid (CPA), specific blockers of the sarcoplasmic/endoplasmic reticulum Ca^{2+}-ATPase (SERCA). After treatment 1 μM TG and 10 μM CPA for 24hours, NTF of PC1 was not detected (**Figure 14**). Especially this cleavage was completely inhibited by TG even if expression level was lower than other conditions. This result shows that cleavage of PC1 is dependent upon altered ER Ca^{2+} homeostasis.

PC1 is constitutively cleaved at His-Leu↓Thr3049 within the GPS domain (17, 41). The best characterized mechanism is the *cis*-autoproteolysis, a self-catalyzed protein rearrangement that results in cleavage at the HX↓(T/S/C)(45). I made mutants of non-cleavable PC1 to confirm cleavage at the GPS domain. Mutagenesis of *PKD1* gene was difficult because of

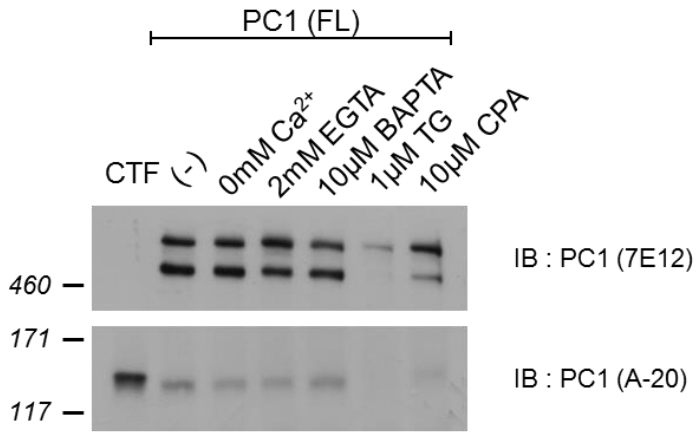

Figure 14. Effect of removal of Ca^{2+} on cleavage of PC1.

HEK 293 cells transfected with hPC1(FL)-flag were treated with reagents to remove intracellular or extracellular Ca^{2+}. HEK 293 cells expressing PC1 treated with Ca^{2+}-free medium, 2 mM EGTA, 10 μM BAPTA, 1 μM TG, and 10 μM CPA were immunoblotted using anti-PC1 (7E12) and anti-PC1 (A-20) antibodies. Cleavage of PC1 was blocked by treatment with 1 μM TG, and 10 μM CPA, specific inhibitors of SERCA. NTF and CTF of PC1 were not detected by antibodies in upper and lower blots.

the large transcript and complex reiterated gene region. To overcome this problem, I considered different ways of approach. Figure 15 shows the process of making mutants. *PKD1*$_{8885-9401bp}$, containing GPS domain, was produced by digestion of pCI-neo hPC1 (FL) with BamHI-KpnI and subcloned into pEGFP-N1. The product was subsequently mutated, digested with the same enzymes, and finally cloned into pCI-neo vector. I examined the role of consensus HLT sequence for cleavage by site-specific mutagenesis (Figure 16A). Such a mechanism of *cis*-autoproteolysis requires that only Thr, Ser, and Cys, which contain a nucleophile side chain (-OH or -SH group), can support cleavage. I found that this was indeed the case. Substitution of Thr by Ser or Cys did not disrupt the cleavage. In contrast, substitution of Thr to Val, Gly, or Arg and deletion of GPS domain blocked cleavage. To confirm correlation between cleavage and pathologic mutations affecting the sequence at or near GPS, I tested two germline mutants (L2993P and Q3016R). I found that each of the mutants almost completely inhibited cleavage (Figure 16B). I confirmed that cleavage occurred at the GPS rather than at another position.

Characterization of PC1 as G protein-coupled receptor (GRCR)

A fundamental property of PC1 is post-translational modification via cleavage at the juxtamembrane GPCR proteolysis site (GPS) motif that is part of the larger GAIN domain (38). The GAIN domain is a defining feature of the adhesion GPCRs (aGPCRs), the second largest subgroup of GPCRs. Also, PC1 C-terminal cytosolic domain has G protein activation region which is defined as a sequence of ≤25 amino acids with consensus motif BB…..BBxB or BB…..BBxxB (B = R, K, or H) (**Figure 17**). It suggests that many signaling pathways from PC1 may be mediated by heterotrimeric G proteins through binding or activation of G proteins (14). Therefore, PC1 may act as a typical GPCR, modulating voltage dependent Ca^{2+} channels and G protein gated K^{+} channels through the activation of $G\alpha_{i/o}$ subunits and the release of $G\beta\gamma$ subunits (15). To identify binding between PC1 and specific $G\alpha$ protein subunits, I utilized heterologous expression of PC1 (CTF) and $G\alpha$ subunits in HEK293 cells by co-immunoprecipitation (co-IP) and FRET imaging (**Figure 18 and 19**). The C-terminal fragment (CTF) of PC1 has C-terminal cytoplasmic tail including G protein activation region and coiled-coil domain

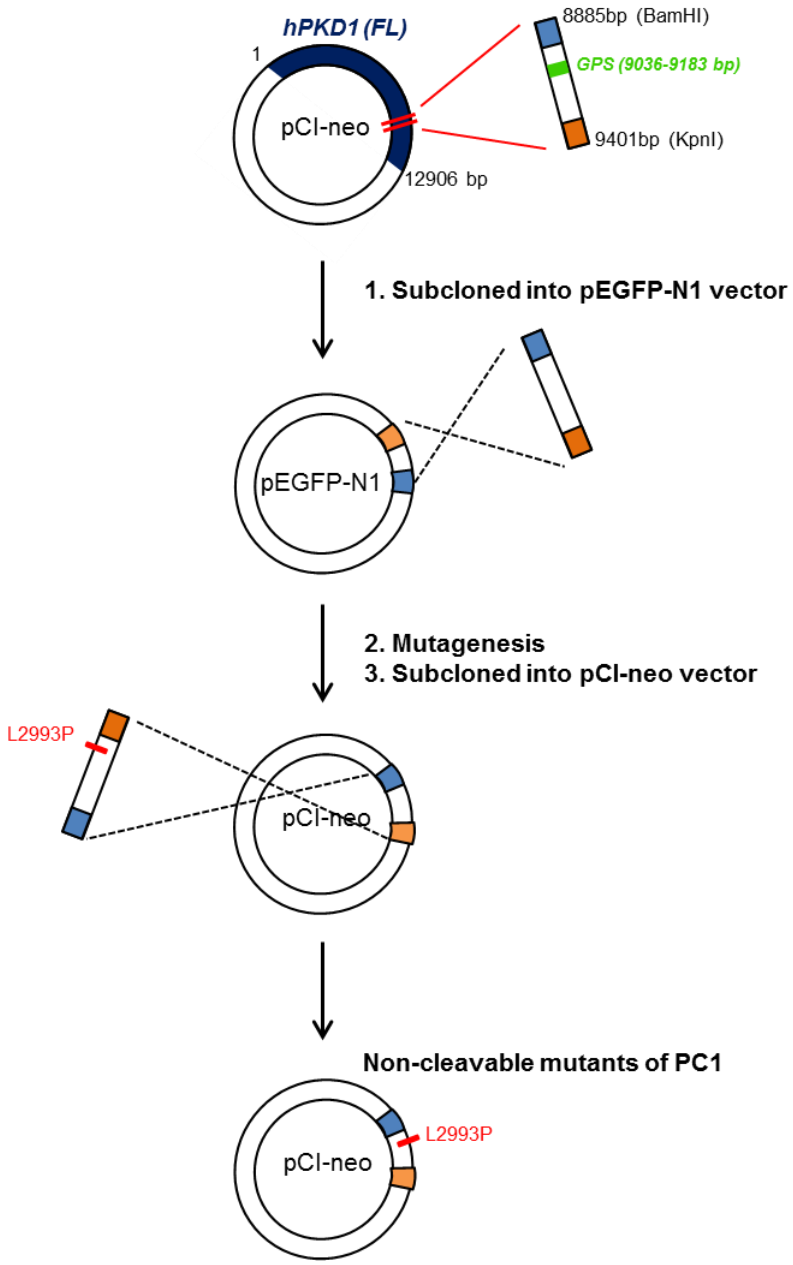
hPKD1 (FL)
1
pCI-neo
12906 bp
8885bp (BamHI)
GPS (9036-9183 bp)
9401bp (KpnI)
1. Subcloned into pEGFP-N1 vector
pEGFP-N1
2. Mutagenesis
3. Subcloned into pCI-neo vector
L2993P
pCI-neo
Non-cleavable mutants of PC1
pCI-neo
L2993P

Figure 15. Cloning process of non-cleavable mutants of PC1.

A fragment of human *PKD1* (8885-9401 bp), containing a G protein proteolytic site (GPS) region (9036-9183 bp), is inserted into a pEGFP-N1 vector using BamHI and KpnI enzyme sites (step 1). The QuikChange site-directed mutagenesis utilizes a pEGFP-N1 hPC1 (8885-9401 bp) and two synthetic oligonucleotide primers containing the desired mutations (e.g. L2993P). The oligonucleotide primers, each complementary to opposite strands of the vector, are extended during temperature cycling by *Pfu* DNA polymerase (step 2). The fragment containing a mutated gene is subcloned into original vector (pCI-neo vector) using the same enzymes (BamHI/KpnI) (step 3).

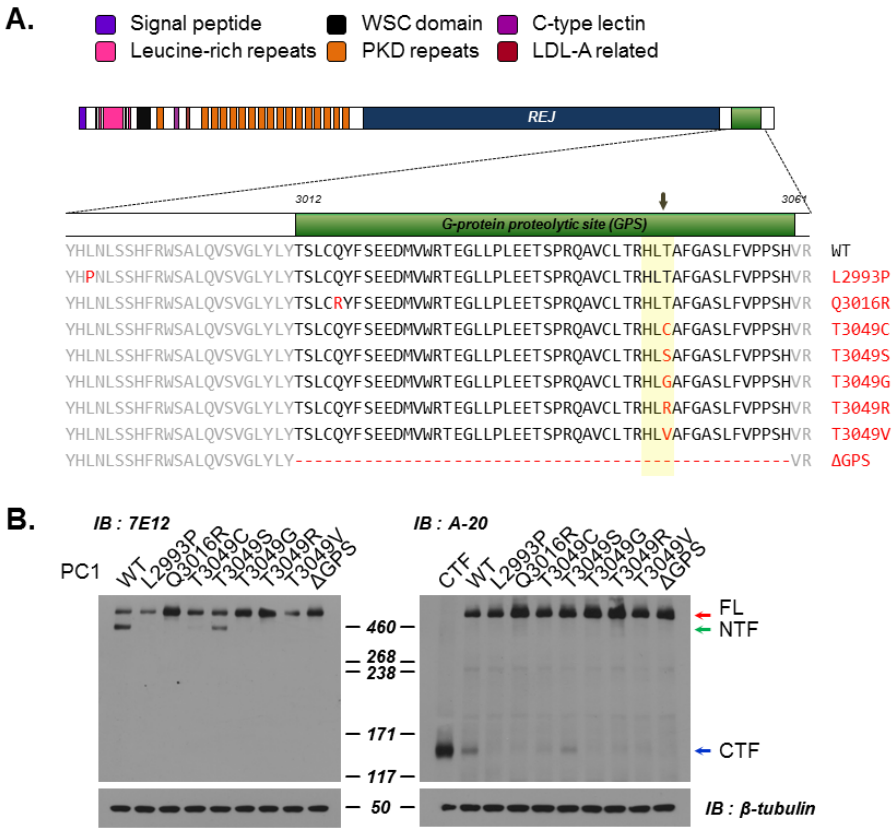
A.
Signal peptide
Leucine-rich repeats
WSC domain
PKD repeats
C-type lectin
LDL-A related
REJ
3012
3061
G-protein proteolytic site (GPS)
YHLNLSSHFRWSALQVSVGLYLYTSLCQYFSEEDMVWRTEGLLPLEETSPRQAVCLTRHLTAFGASLFVPPSHVR WT
YHPNLSSHFRWSALQVSVGLYLYTSLCQYFSEEDMVWRTEGLLPLEETSPRQAVCLTRHLTAFGASLFVPPSHVR L2993P
YHLNLSSHFRWSALQVSVGLYLYTSLCRYFSEEDMVWRTEGLLPLEETSPRQAVCLTRHLTAFGASLFVPPSHVR Q3016R
YHLNLSSHFRWSALQVSVGLYLYTSLCQYFSEEDMVWRTEGLLPLEETSPRQAVCLTRHLCAFGASLFVPPSHVR T3049C
YHLNLSSHFRWSALQVSVGLYLYTSLCQYFSEEDMVWRTEGLLPLEETSPRQAVCLTRHLSAFGASLFVPPSHVR T3049S
YHLNLSSHFRWSALQVSVGLYLYTSLCQYFSEEDMVWRTEGLLPLEETSPRQAVCLTRHLGAFGASLFVPPSHVR T3049G
YHLNLSSHFRWSALQVSVGLYLYTSLCQYFSEEDMVWRTEGLLPLEETSPRQAVCLTRHLRAFGASLFVPPSHVR T3049R
YHLNLSSHFRWSALQVSVGLYLYTSLCQYFSEEDMVWRTEGLLPLEETSPRQAVCLTRHLVAFGASLFVPPSHVR T3049V
YHLNLSSHFRWSALQVSVGLYLY----------VR ΔGPS
B.
IB : 7E12
IB : A-20
PC1
WT
L2993P
Q3016R
T3049C
T3049S
T3049G
T3049R
T3049V
ΔGPS
CTF
460
268
238
171
117
50
FL
NTF
CTF
IB : β-tubulin

Figure 16. Effect of amino acid substitutions on proteolytic cleavage of PC1. (A) Schematic structure of PC1 N-terminal domain. All domains are shown by color boxes. PC1 cleavage occurs at HL↓T^{3049} site in the GPS domain. The cleavage site is marked by an arrow. Two germline mutants (L2993P and Q3016R), substitution of 3049 Thr (T) by Cys (C), Ser (S), Gly (G), Arg (R), and Val (V), and deletion of GPS domain were generated using QuickChange site-directed mutagenesis. (B) HEK 293 cells were transfected with hPC1 (FL)-flag constructs containing missense mutations and assayed for cleavage as shown. Cell lysates were immunoblotted with anti-PC1 (7E12) (left) and anti-PC1 (A-20) (right) antibodies. Mutations T3049C and T3049S did not prevent cleavage of PC1.

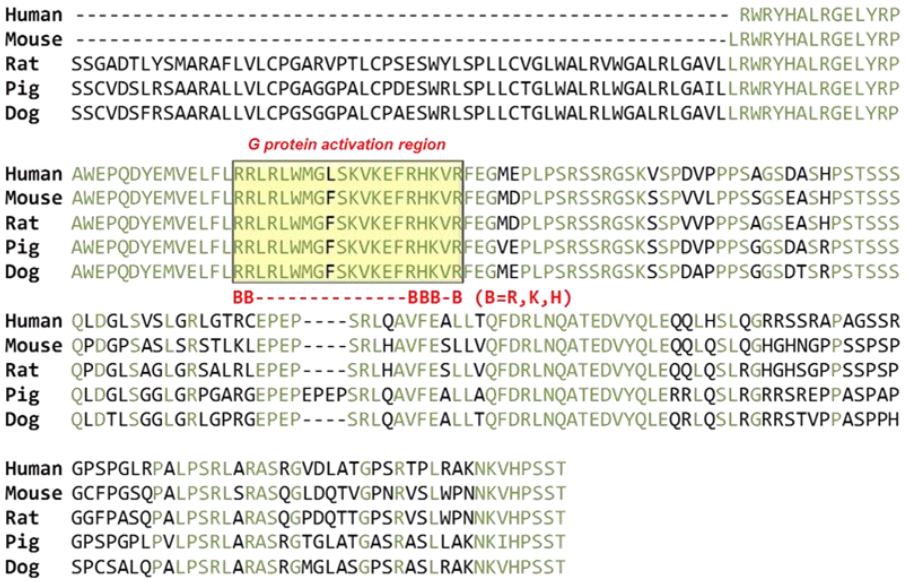

Figure 17. Alignment of amino acid sequences of PC1 C-terminal cytoplasmic tail among many species.

The G protein activation region of PC1 was conserved. It is shown highlighted by the yellow shading

because it cannot receive cleavage signaling through N-terminal extracellular region. I first confirmed the association between PC1 and Gα subunits, by a combination of immunoprecipitation (IP) and Western blot with use of anti-PC1 (A-20), a polyclonal antibody against the C-terminus of human PC1. Protein was immunoprecipitated with anti-PC1 antibody (A-20) then probed with anti-Gα antibodies. The IP band was observed only in the co-expression of PC1 (CTF) with Gα_{i3}, indicating that PC1 specifically interacts with Gα_{i3} (**Figure 18**). I measured the FRET efficiency between PC1 and Gα_{i} by comparing Gα_{i3} with Gα_{i1} or Gα_{i2}. When co-transfected with CFP-tagged PC1 (CTF) and YFP-tagged Gα_{i}, the highest FRET efficiency was recorded in between PC1 (CTF) and Gα_{i3} (**Figure 19**). These results indicated that the PC1 is able to bind to specific G protein subunits; thus, it is likely to act as the GPCR in cells and tissues in which it is expressed.

The activation of TRPC4β channel by Gα_{i}

TRPC4 and TRPC5 channels are nonselective cation channels and modulated by GPCRs (46). It has been reported that TRPC4β expressed in HEK293 cells have a basal activity and

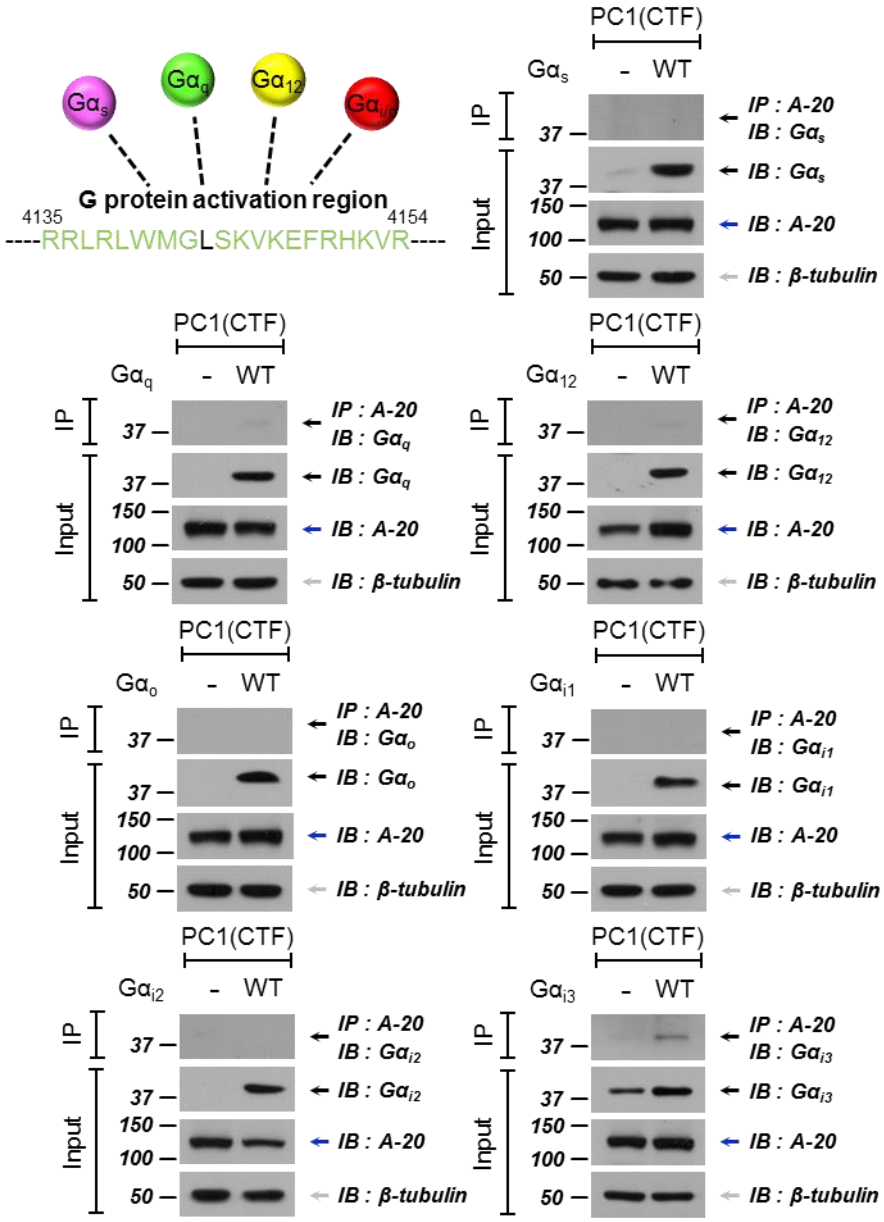
Gαs
Gαq
Gα12
Gαi/o
G protein activation region
4135
4154
----RRLRLWMGLSKVKEFRHKVR----
PC1(CTF)
- WT
IP
Input
37
150
100
50
IP : A-20
IB : Gαs
IB : Gαq
IB : Gα12
IB : Gαo
IB : Gαi1
IB : Gαi2
IB : Gαi3
IB : A-20
IB : β-tubulin

Figure 18. Interaction between Gα subtypes and PC1 (CTF).

The G protein activation region of PC1 C-terminal tail is conserved among many species (4135-4154 amino acid of human PC1). Gα protein classes are defined based on the sequence and function of their alpha subunits, which in mammals fall into several subtypes: Gα_s (magenta), Gα_q (green), Gα_{12} (yellow), and G$\alpha_{i/o}$ (red). Gα subtypes and PC1 (CTF) were co-expressed in HEK 293 cells. 500 μg of proteins from each condition were subjected to immunoprecipitation with anti-PC1 antibody (A-20) and probed with antibody against Gα proteins. PC1 (CTF) interacts directly with Gα_{i3} but not with other Gα subtypes.

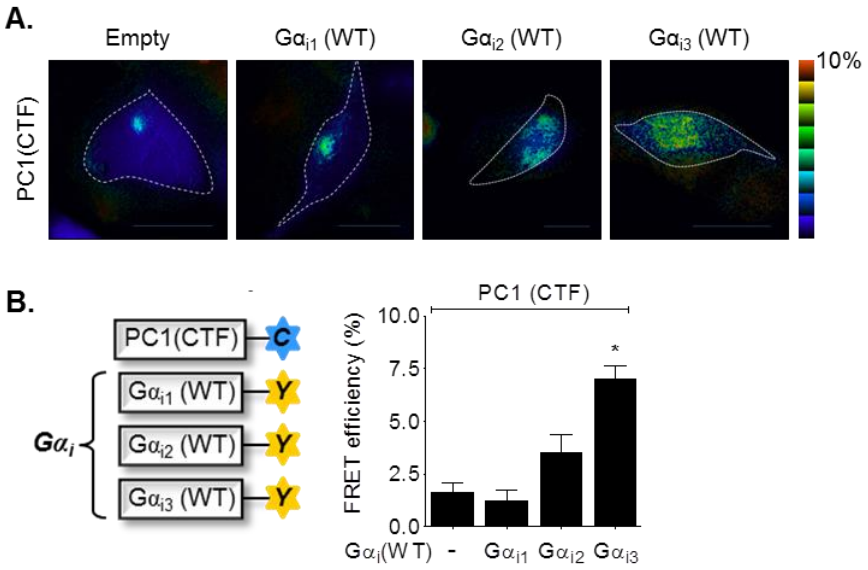

Figure 19. FRET-detectable interactions between PC1 (CTF) and Gα_i subtypes. (A) Representative FRET image of hPC1(CTF)-ECFP co-expressed with G$\alpha_{i\ 1}$(WT)-, G$\alpha_{i\ 2}$(WT)-, and G$\alpha_{i\ 3}$(WT)-EYFP compared to empty vector (pEYFP-N1) expression. (B) A bar graph of FRET efficiency between PC1 (CTF) and Gα_i subtypes.

measurements of TRPC4β activity can be manipulated by altering the extracellular ion composition. In order to efficiently measure TRPC4β activity, I used 140 mM Cs^+-rich solution (**Figure 20A**). The muscarinic acetylcholine receptor M2 which is primarily coupled with Gα_i is one of the well-established G protein-coupled receptors. To investigate the effect of M2 stimulation on TRPC4β, I recorded TRPC4β after treatment with 100 μM Carbachol (CCh) which binds and activates the acetylcholine receptor. TRPC4β current was increased by CCh (266±16 pA/pF) (**Figure 20B and 20C**). Next, to confirm that Gα_i isoforms is involved in the activation of TRPC4β, I used constitutive active form of Gα_i protein (Gα_i CA). TRPC4β was activated to a different extent by all wild type and constitutive active Gα_i isoforms (**Figure 21**).

The activation of TRPC4β channel by PC1

As I've seen, PC1 is considered as an atypical GPCR and TRPC4β can be activated by GPCR. Thus, to investigate whether PC1 affects TRPC4β channel currents, I co-expressed PC1 (FL) or PC1 (CTF) with TRPC4β. Under Cs^+-

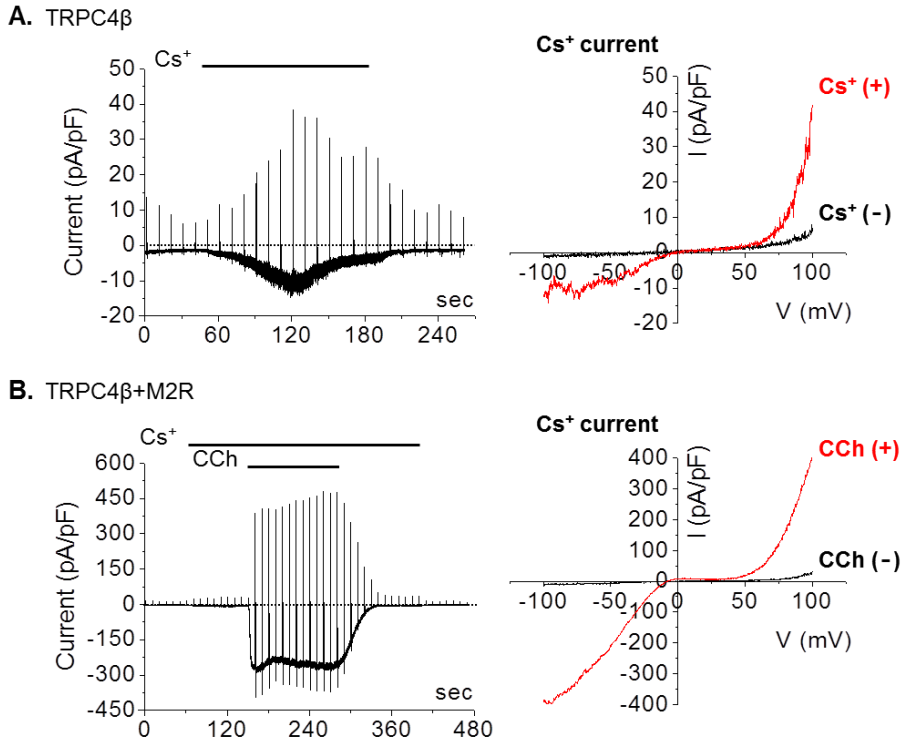

Figure 20. Activation of TRPC4β by the muscarinic acetylcholine receptor M2 with endogenous G$\alpha_{i/o}$.

(A) Expression of TRPC4β alone shows a significant basal current. It is recorded by voltage ramp pulse of +100 to −100 mV during 500 ms durations, whereas the cells are held at −60 mV. (B) Representative current trace of TRPC4β induced by 100 μM carbachol (CCh) after co−expression with the M2 receptor (left). I−V curve of a typical doubly rectifying TRPC4β by CCh−stimulated G$\alpha_{i/o}$ (right). (C) A bar graph of TRPC4β current amplitude by CCh at −60 mV.

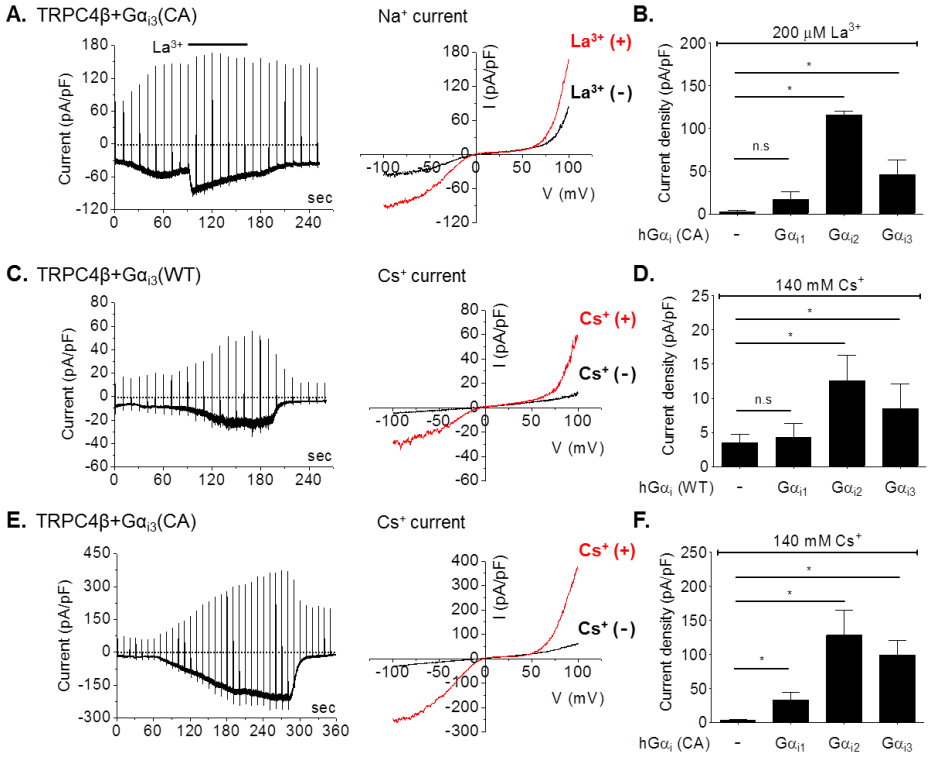
A. TRPC4β+Gαi3(CA)
La3+
Current (pA/pF)
sec
Na+ current
La3+ (+)
La3+ (-)
I (pA/pF)
V (mV)
B.
200 μM La3+
Current density (pA/pF)
n.s
hGαi (CA)
-
Gαi1
Gαi2
Gαi3
C. TRPC4β+Gαi3(WT)
Cs+ current
Cs+ (+)
Cs+ (-)
D.
140 mM Cs+
hGαi (WT)
E. TRPC4β+Gαi3(CA)
F.

Figure 21. Effect of $G\alpha_i$ isoforms on TRPC4β activity.

Here and in all other figures to measure TRPC4β activity, the current was recorded in TRPC4β-expressing HEK 293 cells. The typical I-V relationship is shown before (black) and after maximal current (red) activation. The bar graphs list the mean ± s.e.m. of current density (pA/pF) at -60 mV. * p <0.05 and n.s. not significant. (A) Represent Na^+ current trace of TRPC4β activated by 200 μM La^{3+} after co-expression with the constitutively active $G\alpha_{i3}$ ($G\alpha_{i3}$ (CA)). (C) Representative Cs^+ current trace of TRPC4β activated by $G\alpha_{i3}$ (WT). (E) Representative Cs^+ current trace of TRPC4β induced by $G\alpha_{i3}$ (CA). (B), (D), and (F) A bar graph of TRPC4β current amplitude by $G\alpha_i$ isoforms.

rich solution, TRPC4β current was increased by FL (41±14 pA/pF) but not CTF (7±3 pA/pF) compared to the control (4± 1 pA/pF) (**Figure 22A and 22B**). To efficiently measure TRPC4 β activity, I used a 140 mM Cs^+-rich solution on the basis of the high permeability of Cs^+ ion in TRPC4 (47). Next, GTPγ S-induced Cs^+ current of TRPC4β by FL or CTF made no difference, because intracellular application of GTPγS which activates different types of G proteins through the patch pipette fully activated TRPC4β (**Figure 22C and 22D**). These results suggest that Gα proteins signaling through cleavage of PC1 is necessary to activate TRPC4β. Also, the channel activity was regulated by PC1 without increase in surface expression (**Figure 23**). I measured intracellular Ca^{2+} level using Fura-2 in **Figure 24**. PC1 (FL) increased TRPC4β-mediated Ca^{2+} influx. **Figure 25** showed that TRPC4β current was inhibited by a dominant negative form of Gα_{i3} protein (Gα_{i3} G202T) in cells transfected with PC1 (FL). This result indicates that activation of TRPC4β by PC1 is mediated by Gα_{i3} among Gα protein subfamily.

I also confirmed whether TRPC4β is activated by PC1 using non-cleavable mutants. As discussed earlier, CTF form of PC1

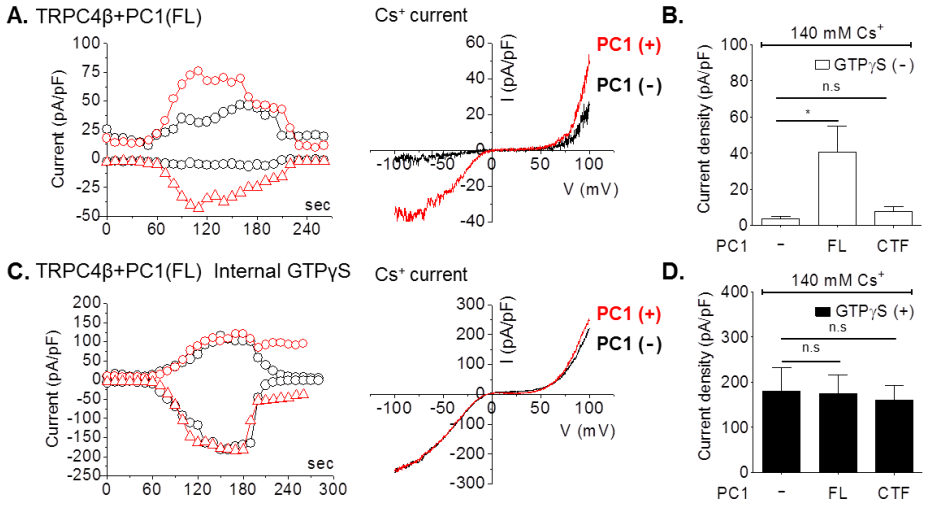

Figure 22. Activation of TRPC4β by PC1 (FL).

(A) HEK 293 cells were co-transfected with TRPC4β and PC1 (FL). The I-V curve was taken before (black) and after (red) the co-transfection with PC1 (FL). (C) The current was recorded in TRPC4β/PC1(FL) co-transfected HEK 293 cells and infused with GTPγS. The I-V curve was taken before (black) and after (red) the co-transfection with PC1 (FL). (B) and (D) The bar graphs list the mean ± s.e.m of current density (pA/pF) at −60 mV in the absence (B) or presence (D) of GTPγS infusion.

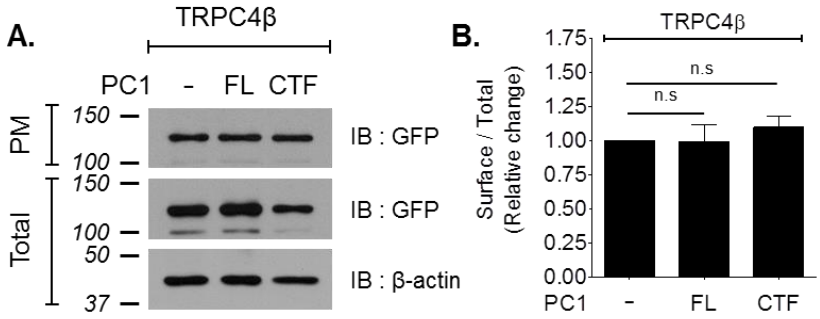

Figure 23. Surface expression of TRPC4β by PC1.

(A) Representative cell surface biotinylation assay showing surface (PM) and total expression of TRPC4β as indicated after co-expression with PC1 (FL) or PC1 (CTF). Biotinylated and total cellular proteins were quantified by immunoblot analysis. Surface expression of TRPC4β by PC1 was not altered. (B) A bar graph showing densitometric analysis of 3 repetitions of this experiment.

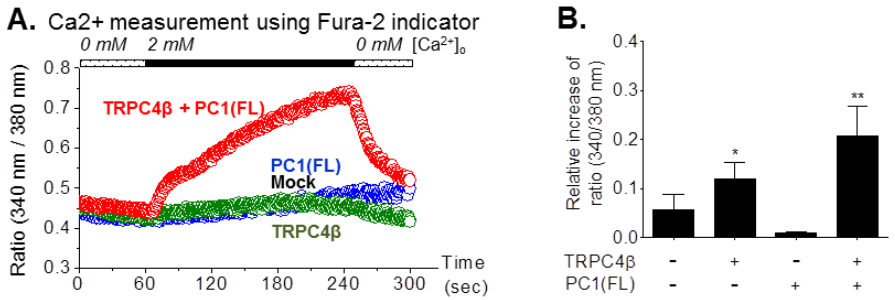

Figure 24. $[Ca^{2+}]_i$ measurements in PC1-mediated activity of TRPC4β. (A) Cytoplasmic calcium measurements in cells expressing TRPC4β alone or co-expressing PC1 (FL) loaded with Fura-2 (ratiometric measurement at 340 nm and 380 nm, expressed as 340/380). The cells were perfused with an extracellular solution containing no added calcium, and then extracellular calcium was increased to 2 mM for 3 minutes. (B) A bar graph shows that calcium influx increases in TRPC4β channel activated by PC1 (FL).

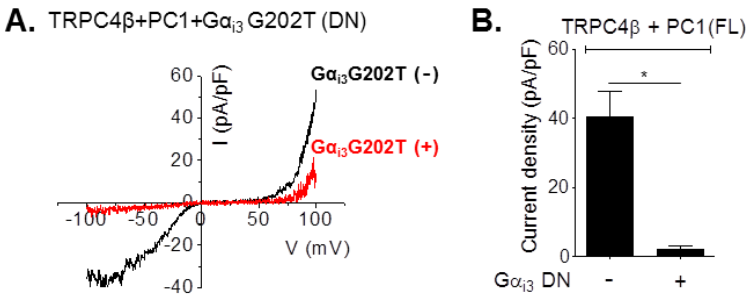

Figure 25. Inhibition of PC1-mediated TRPC4β activity by dominant negative Gα_{i3}.

(A) HEK 293 cells were transfected with TRPC4β, PC1 (FL), and Gα_{i3} G202T (dominant negative Gα_{i3}). The I-V relationship is shown before (black) and after maximal current (red) inhibition. (B) A bar graph of TRPC4β current amplitude by Gα_{i3} (DN) at −60 mV. Statistical significance was denoted by an asterisk (*, $p<0.05$).

did not affect TRPC4β activity. In accord with this, non-cleavable mutants (L2993P, Q3016R and T3049G/R/V) did not activate TRPC4β channel. In contrast, I observed activity of TRPC4β in cells transfected with T3049C or T3049S which occur normal cleavage(**Figure 26**).

PC1 is likely to function as a receptor for Wnt ligands to induce Ca^{2+} influx (48). Wnts bind to the extracellular domain of PC1 and induce whole-cell currents. Thus, I tested whether PC1-mediated TRPC4β activity increase in response to Wnt9b. As shown in **Figure 27**, addition of Wnt9b (500 ng/ml) did not affect the activity of TRPC4β by PC1 and cleavage.

Taken together, these data lead me to conclude that PC1 and TRPC4β can form a receptor-channel complex.

STATs phosphorylation by PC1-mediated activity of TRPC4β

PC1 has been implicated in a variety of intracellular signaling events including JAK-STAT signaling. Overexpression of full-length PC1 can activate signal transducer and activator of transcription 1 (STAT1), STAT3 and STAT6 (10, 21, 49) which are mediated in signaling such as proliferation, differentiation and death. STATs are phosphorylated and

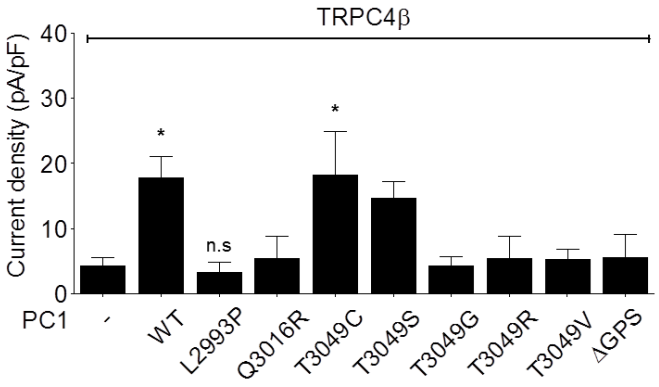

Figure 26. Activity of TRPC4β by non-cleavable PC1 mutants.

HEK 293 cells were transfected with TRPC4β and wild-type or non-cleavable mutants of PC1 (FL). The bar graphs list the mean ± s.e.m. of current density (pA/pF) at −60 mV of the indicated number of experiments. * $p<0.05$ and n.s. not significant.

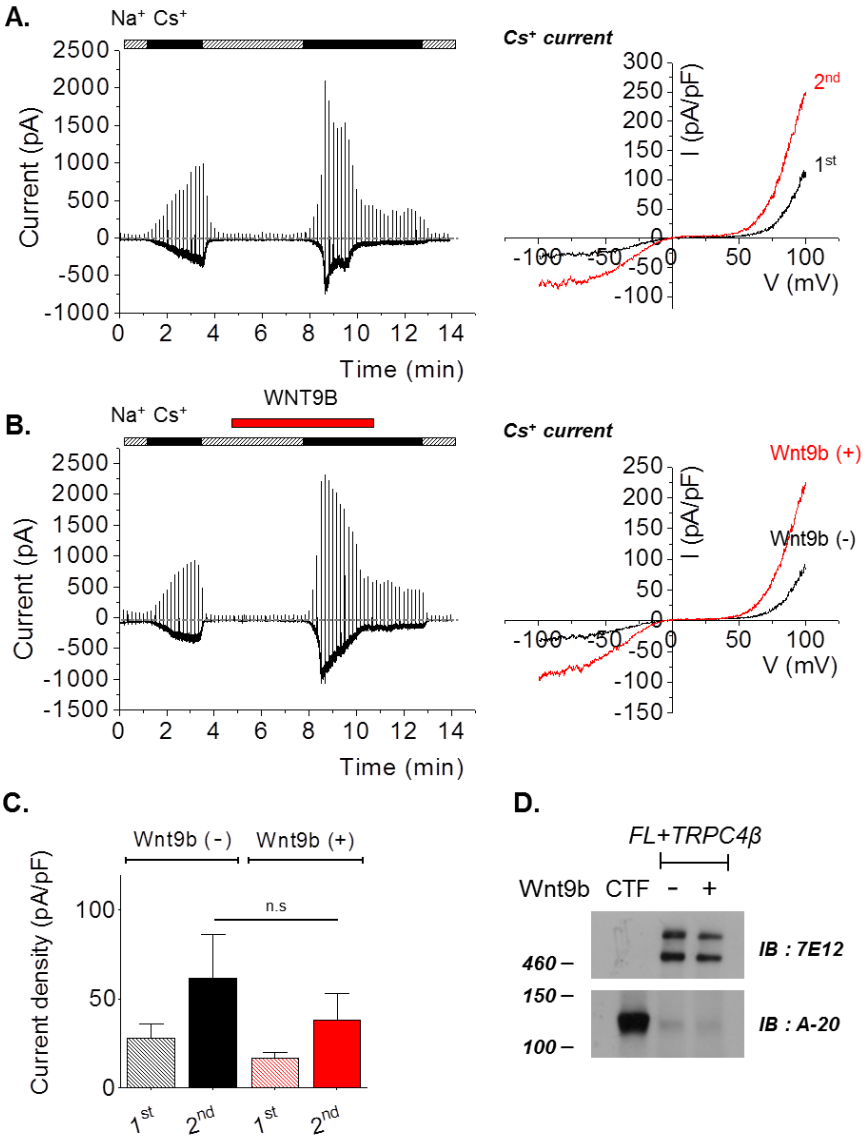
A.
Na+ Cs+
Current (pA)
Time (min)
Cs+ current
I (pA/pF)
V (mV)
2nd
1st
B.
WNT9B
Na+ Cs+
Current (pA)
Time (min)
Cs+ current
Wnt9b (+)
Wnt9b (-)
I (pA/pF)
V (mV)
C.
Wnt9b (-)
Wnt9b (+)
n.s
Current density (pA/pF)
1st
2nd
1st
2nd
D.
FL+TRPC4β
Wnt9b CTF - +
460 –
150 –
100 –
IB : 7E12
IB : A-20

Figure 27. Effect of Wnt9b on PC1−mediated TRPC4β activity.

(A) Representative current trace of TRPC4β activated by PC1 (FL). The current was recorded in TRPC4β/PC1 (FL) co−transfected HEK 293 cells. (B) Representative current trace of Wnt9b−induced TRPC4β/PC1 (FL). The current was recorded in TRPC4β/PC1 (FL) co−transfected HEK 293 cells. The I−V curve was taken before (black) and after (red) the addition of 500 ng/ml Wnt9b. In all panels, basal solutions were applied at the time indicated by the *bars* (Na^+; gray and Cs^+; black). (C) A bar graph showing activation of PC1 (FL)−mediated TRPC4β treated with or without Wnt9b (500 ng/ml). n.s, indicates no significance. (D) Identification of PC1 cleavage by Wnt9b. HEK 293 cells were co−transfected with TRPC4β and PC1 (FL) and incubated with Wnt9b in the presence or absence for 18h. Western blot analysis was performed with the indicated antibodies.

activated by protein tyrosine kinases, including growth factor receptors, such as EGFR, and non-receptor tyrosine kinases (Src and JAK)(50). To investigate whether STATs activation by PC1 was regulated dependently on Src kinase activity, I transiently transfected HEK 293 cells with dominant-negative Src (Src^{DN}) mutants. As shown in **Figure 28A and 28B**, STAT1 and STAT3 was activated by PC1 and wild-type Src (Src^{WT}), respectively. The basal activity of STAT1 and STAT3 was not changed by Src^{DN}. The co-expression of PC1 and Src^{WT} increased further STAT1 and STAT3 levels. Activation of STAT1 and STAT3 by PC1 was not affected by Src^{DN}. These results suggest that PC1 leads to Src-independent activation of STAT1 and STAT3 through tyrosine phosphorylation. Next, I observed whether activation of TRPC4β channel by PC1 affects STATs phosphorylation. Activation of STAT1 and STAT3 was further increased by PC1-mediated activity of TRPC4β (**Figure 29A and 29B**). In addition, it has been reported that CTT of PC1 is released by γ-secretase-mediated cleavage (44). I confirmed whether levels of STAT phosphorylation through PC1-mediated TRPC4β activity is inhibited by γ-secretase inhibitor DAPT (**Figure 30**).

Transfection mixtures of PC1 or/and TRPC4β were added drop wise to cell culture media containing 80 μM DAPT and incubated for 24 hours. STATs activity of PC1/TRPC4β was inhibited by DAPT, indicating that STATs phosphorylation is associated with cleavage of PC1 (CTT). To investigate the potential role of Ca^{2+} entry through TRPC4β channel in increased STATs phosphorylation, I observed the effect of removing extracellular calcium ions using Ca^{2+}-free medium. The increased levels of STAT1 and STAT3 were significantly attenuated in Ca^{2+}-free medium, compared with normal condition (**Figure 31A and 31B**). The activation of STAT3 was more susceptible to PC1-induced calcium influx than STAT1. These results show that calcium is required to activate STATs and more complicated interaction between PC1 and TRPC4β channel for phosphorylated STAT1 might exist compared with phosphorylated STAT3.

NFATs dephosphorylation by PC1-mediated activity of TRPC4β

PC1 is involved in regulating intracellular Ca^{2+} levels (11, 51). Transient intracellular Ca^{2+} increases are associated with cellular functions such as muscle contraction, synaptic

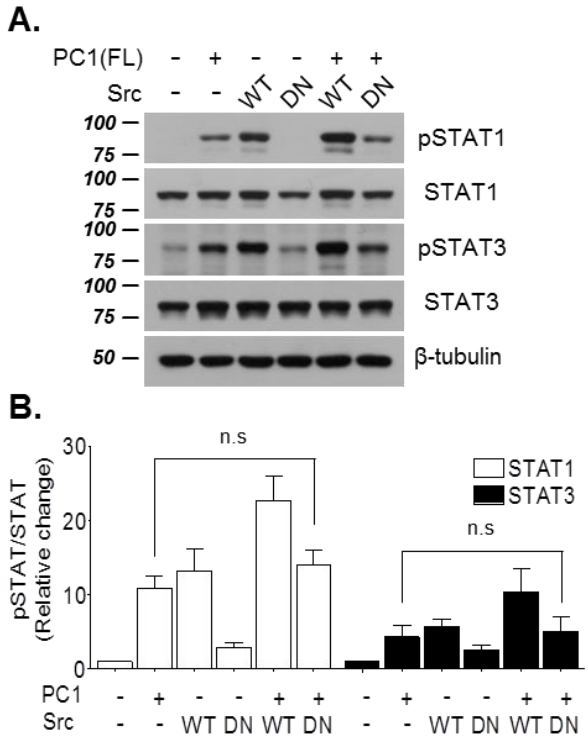

Figure 28. Effect of Src kinase on STATs phosphorylation.

(A) HEK 293 cells were transfected with PC1 (FL) and/or wild-type or dominant-negative Src. Cell lysates were used for Western blot analysis with antibodies against total and phosphorylated STAT1 and STAT3. (B) A bar graph shows mean levels of phosphorylated STATs relative to total STATs protein. n.s. not significant.

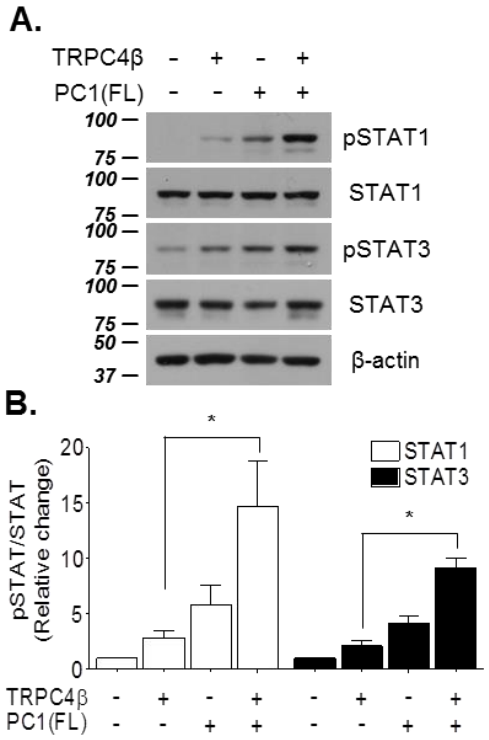

Figure 29. STATs phosphorylation by PC1-mediated TRPC4β signaling. (A) HEK 293 cells were transfected with PC1 (FL) and/or TRPC4β. Level of pSTAT1, STAT1, pSTAT3, and STAT3 were assessed by Western blotting. (B) Quantification of Western blotting images by Image J. Data is representative of four experiments. A bar graph shows mean levels of phosphorylated STATs relative to total STATs protein. Statistical significance was denoted by an asterisk (*, $p<0.05$).

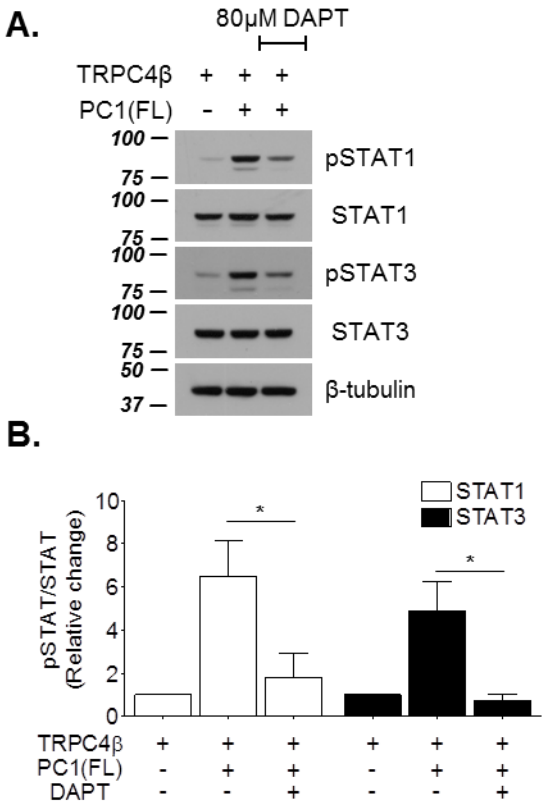

Figure 30. STATs phosphorylation by γ-secretase inhibitor. (A) HEK 293 cells were transfected with PC1 (FL) and/or TRPC4β. The γ-secretase inhibitor DAPT (80μM) was added to the media. Level of pSTAT1, STAT1, pSTAT3, and STAT3 were assessed by Western blotting. (B) Quantification of Western blotting images by Image J. Data is representative of three experiments. A bar graph shows mean levels of phosphorylated STATs relative to total STATs protein. Statistical significance was denoted by an asterisk (*, $p<0.05$).

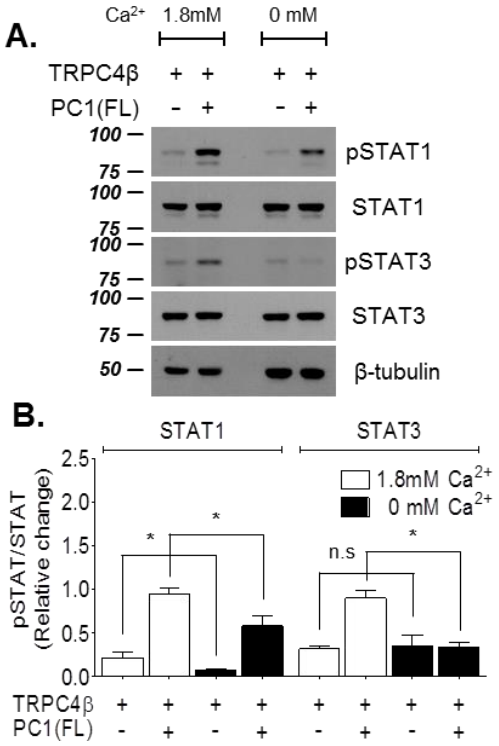

Figure 31. Effect of Ca^{2+} on STATs phosphorylation by PC1/TRPC4β. (A) HEK 293 cells were transfected or co-transfected with TRPC4β and PC1 (FL). After transfection, extracellular calcium ions were removed using Ca^{2+}-free medium. Level of pSTAT1, STAT1, pSTAT3, and STAT3 were assessed by Western blotting. (B) Quantification of Western blotting images by Image J. A bar graph shows mean levels of phosphorylated STATs relative to total STATs protein according to calcium change. Statistical significance was denoted by an asterisk (*, $p<0.05$). n.s. not significant.

transmission, and neuroendocrine secretion. In contrast, sustained Ca^{2+} signals are known to affect transcriptional events leading to adaptive cellular changes and to changes in cell proliferation and cell differentiation (52, 53). A cellular target for sustained increases in Ca^{2+} is calcineurin, a ubiquitous serine-threonine phosphatase. An important intracellular substrate for calcineurin is nuclear factor of activated T-cells (NFAT).

To determine whether PC1-mediated TRPC4β activation can induce calcineurin/NFAT signaling, I co-expressed a combination of PC1 and TRPC4β with an NFAT promoter luciferase reporter construct. The promoter activity was analyzed by a luciferase assay. Co-expression of PC1 (FL) and TRPC4β elevated NFAT luciferase reporter activity by ~2 fold as compared with the transfection with either PC1 (FL) or TRPC4β, whereas NFAT activity by PC1 (CTF) and TRPC4β showed no significant changes (**Figure 32A**). Because calcineurin activation and Ca^{2+} flux are signaling upstream of NFAT activation, I tested whether the PC1/TRPC4β /calcineurin/NFAT signaling pathway could be blocked by cyclosporin A (CsA), an immune suppressive agent which

specifically inhibits calcineurin activation. Addition of 1 μM of CsA to the culture inhibited PC1/TRPC4β-mediated NFAT activation by ~90% (**Figure 32B**). NFAT activity was also attenuated in Ca^{2+}-free medium (**Figure 32C**). NFAT transcription factor family consists of five members (NFATc1-C4 and NFAT5). NFATc1 through NFATc4 are regulated by Ca^{2+} signaling and are calcineurin-sensitive (54). As shown in **Figure 32D**, the presence of all four NFATs was confirmed at the protein level by Western blotting. Multiple bands likely indicate the presence of different isoforms and phosphorylation states. NFATc4 was differentially dephosphorylated by PC1-mediated activation of TRPC4β. Collectively, these results indicate that Ca^{2+} influx through PC1 stimulated TRPC4β channel activates the NFAT signaling pathway and NFATc4 is the only necessary isoform.

Regulation of endothelial functions by PC1-mediated activity of TRPC4β

TRPC subfamily plays a role in normal and pathophysiological vascular function (55, 56). TRPCs are involved in vascular tone (e.g., TRPC4, TRPV1, and TRPV4), regulation of vascular

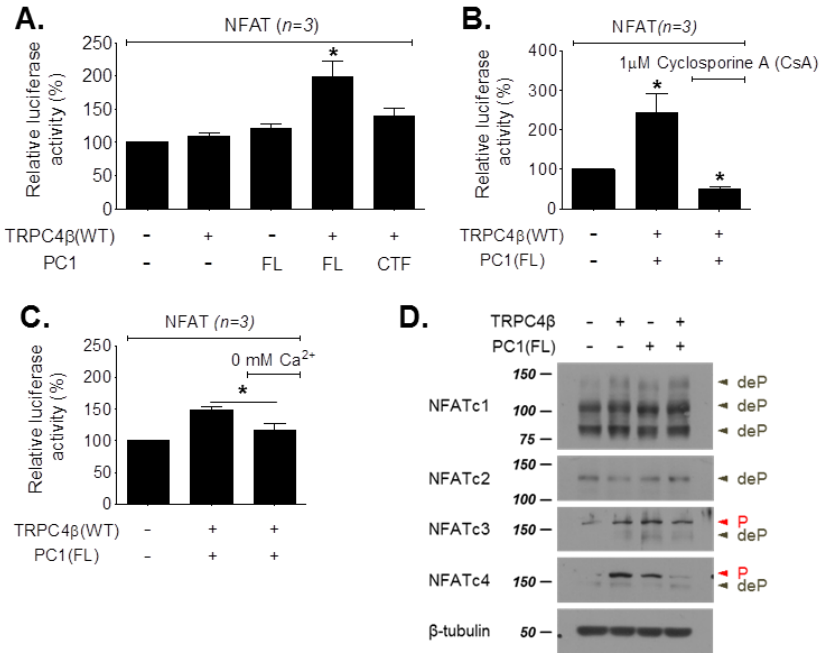

Figure 32. Luciferase reporter assay of NFAT.

(A) HEK 293 cells were transfected with NFAT-Luc reporter construct and/or TRPC4β and PC1 for 24h prior to luciferase activity assay. The luciferase activity was expressed as a relative value compared to that of the untreated cells which was set to 100%. (B) Cells were treated with 10 μM CsA for 24h prior to each analysis. TRPC4β/PC1-mediated luciferase activity was inhibited by CsA. (C) Extracellular calcium ions were removed using Ca^{2+}-free medium. (D) HEK 293 cells were transfected with TRPC4β and/or PC1 (FL). The cell extracts were probed using the indicated antibodies.

permeability (e.g., TRPC1, TRPC4, TRPC6, and TRPV1), hypoxia-induced vascular remodeling (e.g., TRPC4), angiogenesis (e.g., TRPC4 and TRPC6), endothelial cell proliferation, and apoptosis (57). Thus, TRPC4 plays significant roles in the TRPC superfamily. It has been also reported that PC1 has an important role in vascular function. *Pkd1* knock-out mice dies in mid-gestation with a variety of phenotypes including a vasculopathy that is characterized by profound edema (58, 59). In order to investigate the relationship between PC1/TRPC4β pathway and endothelial function,

I first confirmed expression of TRPC4 and PC1 in HUVECs using Western blot analysis. TRPC4β compared to other TRPC4 isoforms was predominantly expressed in endothelial cells (**Figure 33A**). Expression of PC1 was detected previously in endothelial cells (**Figure 12**). In addition, I could identify expression of Gα subtypes which was involved in TRPC4β activation by PC1. Gα_{i3} was expressed in given cell lines (**Figure 33B**). I next examined the silencing effect of TRPC4β and PC1 on HUVEC migration. In wound-healing assays, endothelial cells treated with vehicle were able to close ~100% of the wound. In contrast, endothelial cells treated 20 μM

ML204 were only able to close ~50% of the wound (**Figure 34A**). I found that the migration rate of HUVECs transfected with TRPC4 siRNA was significantly decreased (**Figure 34B**). To identify whether STATs affect endothelial migration, I transfected with STAT1 or STAT3 siRNA into HUVEC. To test siRNAs efficiency, STAT1 and STAT3 transcript levels were evaluated by Western blot. I found that the tested siRNA effectively reduced the levels of STAT1 and STAT3 expression (**Figure 35**). The migration of STAT1 knockdown cells was obviously inhibited. By contrast, STAT3 siRNA did not show any significant difference (**Figure 36**). These results suggest that PC1-mediated TRPC4β activation and STAT1 but not STAT3 play a role in endothelial migration. Thus, mutations of *PKD1* can contribute to endothelial dysfunction.

Adherens junctions have key roles in the maintenance of vascular integrity. The depletion of VE-cadherin-catenin complex induces endothelial barrier dysfunction and has been observed in various vascular disease states. I investigated whether PC1/TRPC4β signaling is involved in the formation of junctions of endothelial cells. I analyzed the subcellular localization of VE-cadherin and its associated protein, β-

catenin, in HUVEC treated with siRNA or ML204 using immunofluorescence. Without stimulation, VE-cadherin and β-catenin was localized at the plasma membrane (**Figure 37A(a) and 37B(a)**). Upon stimulation with PC1 siRNA or/and 20 μM ML204 for 48 hour, VE-cadherin (**Figure 37A(b-d)**) and β-catenin (**Figure 37B(b-d)**) levels diminished at the plasma membrane, presumably because of increased endocytosis or internalization. Additionally, STAT1 knockdown impair cell-cell adhesion by inducing disassembly of the VE-cadherin and β-catenin at junctions in HUVEC (**Figure 37A(e) and 37B(e)**). VE-cadherin and β-catenin at endothelial cell junctions is significantly reduced by down-regulation of PC1 or TRPC4.

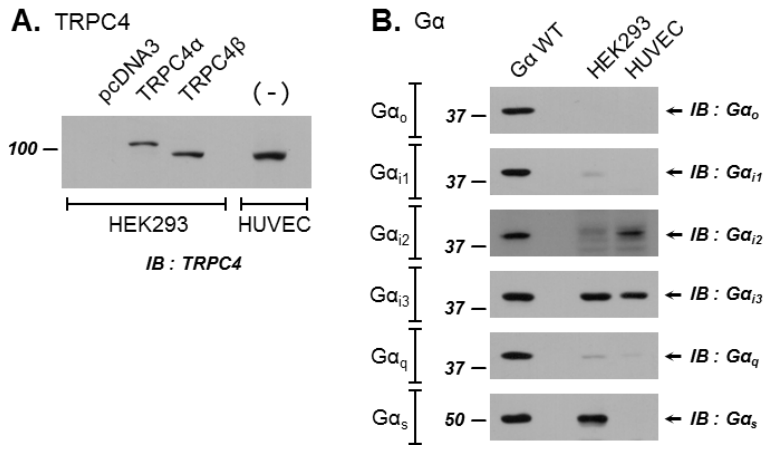

Figure 33. Expression of TRPC4 and Gα proteins in HUVEC.

(A) HEK 293 cells with or without transient transfection of TRPC4α or TRPC4β were immunoblotted with an anti-TRPC4. Endogenous TRPC4β in HUVEC was detected by anti-TRPC4 antibody. (B) HEK 293 cells were transfected with Gα subtypes. Level of Gα proteins were assessed by Western blotting.

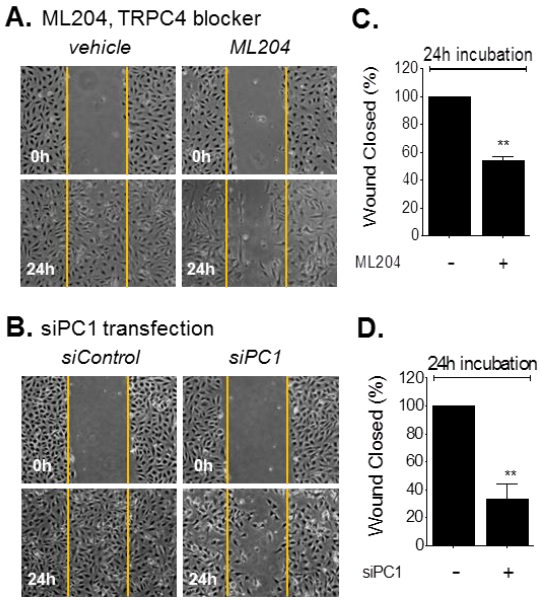

Figure 34. Effects of ML204 treatment and *PKD1* gene silencing on the migration of HUVEC. Wound healing assays were performed on HUVEC in the absence or the presence of the TRPC4 blocker ML204 (20 μM) (A), and siPC1 (B). Movement of cells into wound was shown for ML204 and siPC1 treated cells at 0 and 24h post scratch. The yellow indicated the boundary lines of scratch. Cell migration was assessed by recover of the scratch. (C) and (D) The bar graphs show quantitative data for the cell migration assay. The area of the wound was measured at the two time points in every group, and % reduction of initial scratch area was compared.

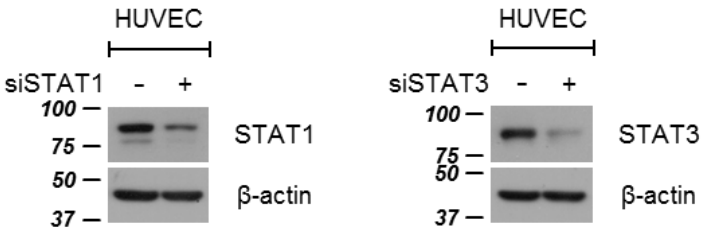

Figure 35. Analysis of siRNA-mediated silencing of STAT1 and STAT3 expression in HUVEC.

HUVECs were transfected with siSTAT1 (left) or siSTAT3 (right) and harvested at 48h post-transfection. Western blot analysis was performed with the indicated antibodies. Expression level of STAT1 and STAT3 protein was reduced by siSTAT1 and siSTAT3, respectively.

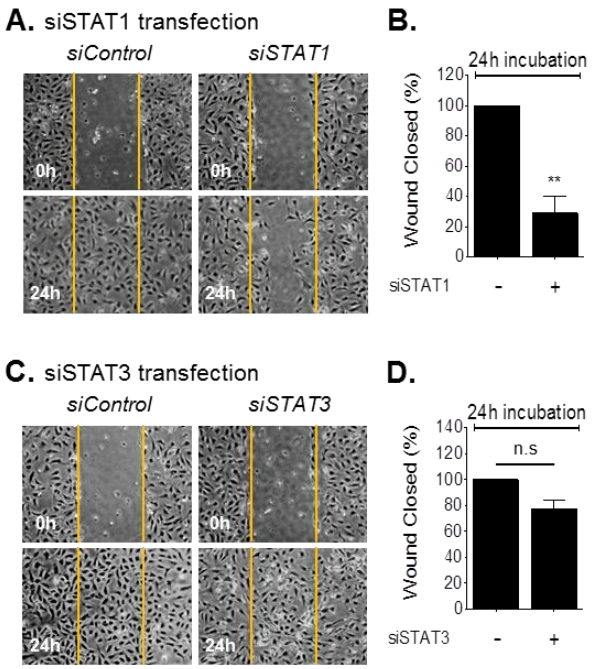

Figure 36. Effects of *STAT1 and STAT3* gene silencing on the migration of HUVEC. Wound healing assays were performed on HUVEC in the absence or the presence of the siSTAT1 (A), and siSTAT3 (B). Movement of cells into wound was shown for siSTAT1 and siSTAT3 treated cells at 0 and 24h post scratch. The yellow indicated the boundary lines of scratch. Cell migration was assessed by recover of the scratch. (C) and (D) The bar graphs show quantitative data for the cell migration assay. The area of the wound was measured at the two time points in every group, and % reduction of initial scratch area was compared.

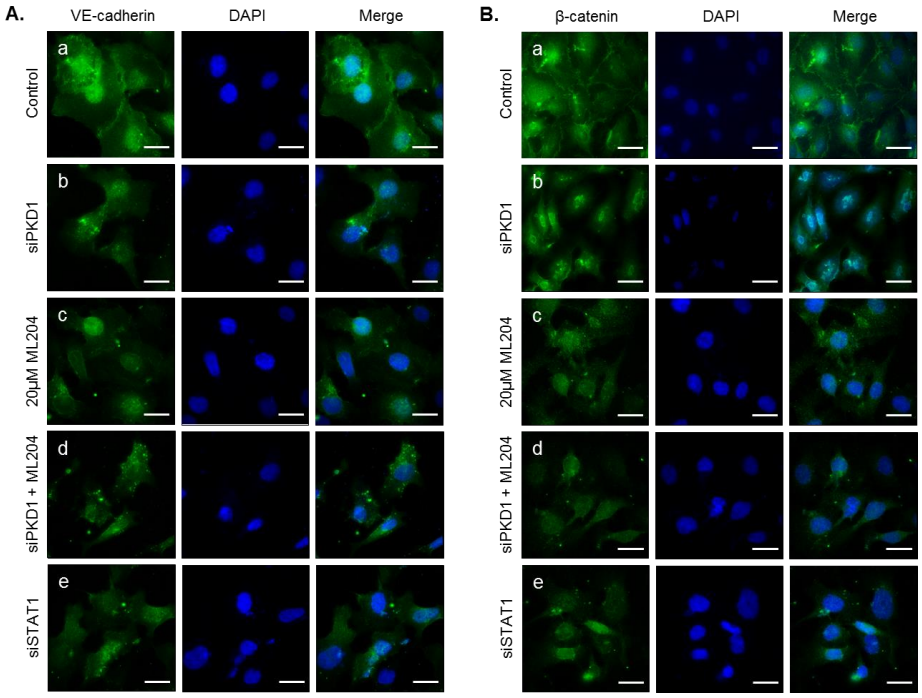

Figure 37. Effect of PC1 and TRPC4 on cell-cell junctions. Immunofluorescence images of cell adherens junction protein VE-cadherin and β-catenin. HUVECs were treated with siRNA or/and 20 μM ML204. Cells were fixed 48h after siRNA transfection and immunostained with antibodies to VE-cadherin (A) and β-catenin (B). (a) control, (b) PC1 siRNA, (c) 20 μM ML204, (d) PC1 siRNA and 20 μM ML204, (e) STAT1 siRNA.

DISCUSSION

I demonstrated that down-regulation of PC1-mediated TRPC4β activity plays a key role in the endothelial migration. My data suggest that TRPC4β can be activated by stimulation of Gα_i-coupled PC1. Several lines of evidence support that PC1 functions as G protein-coupled receptor. First, C-terminal tail of PC1 contains G protein binding region. This region was conserved among the many species. I observed that PC1 specifically interact with Gα_{i3} using co-IP. FRET efficiency between PC1 and Gα_{i3} increased compared to other Gα_i isoforms. Second, PC1 is cleaved at GPS, just before the first transmembrane domain and then leads to G protein mediated signaling cascade. The GPS motif was first identified in a neuronal GPCR, CIRL/latrophilin (60), and has recently been recognized as a part of the larger GPCR autoproteolysis-inducing (GAIN) domain that is also present in PC1. Interestingly, the cleaved PC1 N-terminal fragment remains non-covalently attached to the membrane bound C-terminal fragment (41). Such heterodimer PC1 is required to transduce the signal through G protein and plays an important role for biological function. In contrast, it has been reported that

deletion of the NTF resulted in constitutive activation for some aGPCRs (61), suggesting that NTF association might normally prevent constitutive activation. However, all of the disease associated missense mutations located in the GAIN domain and the adjacent REJ module of PC1 analyzed so far impaired or disrupted cleavage. Defective GPS cleavage of PC1 has been found in a subset of ADPKD patients with aneurysmal rupture (62). I identified loss of the functional properties of PC1 as making non-cleavable mutants of PC1. Third, PC1 is a large integral membrane protein with 11 transmembrane segments and structurally resembles a receptor or adhesion molecule. Thus, these multiple lines of evidence demonstrate that PC1 represents structural or functional characteristics of GPCR.

I show that PC1 can activate TRPC4β channel through Gα protein. It is reported previously that Gα_i proteins play an essential role as novel activators of TRPC4 in my laboratory. First, PC1 (FL) but not PC1 (CTF) activate TRPC4β. PC1 (CTF) does not affect activation of TRPC4β due to loss of N-terminus which mediates G protein signaling through C-terminal tail of PC1. Second, non-cleavable mutants of PC1 do not activate TRPC4β current. Cleavage of PC1 N-terminal or

C-terminal is blocked by missense mutations at GPS domain. Third, I measured intracellular Ca^{2+} level using Fura-2. PC1 (FL) increases Ca^{2+} influx through TRPC4β channel. Fourth, intracellular 0.2 mM GTPγS-induced TRPC4β activation is not significantly different in the presence or absence of PC1. Fifth, activation of TRPC4β by PC1 (FL) is inhibited by dominant negative Gα_{i3}. Therefore, these results demonstrate unambiguously that TRPC4β is activated by Gα_{i3} coupled-PC1.

Next, I identified intracellular signaling cascades through a rise of cytosolic Ca^{2+} by PC1/TRPC4β. Many researches have been reported that disturbance in the balance between cell proliferation and apoptosis causes ADPKD. Abnormal proliferation in tubular epithelial cells plays a crucial role in cyst development and/or growth in PKD (63). The kidneys from patients with ADPKD have high levels of apoptosis as well as cellular proliferation (64). Intracranial aneurysm is also believed to develop as a result of disruption of the balance of cell proliferation and apoptosis (65). Indeed, proliferation and apoptosis should be tightly regulated. Among many regulatory factors of proliferation and apoptosis, I observed activation of

STATs and NFAT by PC1/TRPC4β. STAT1 is dominantly phosphorylated by activation of PC1-mediated TRPC4β. The Ca^{2+} influx can also leads to phosphorylation of STAT1 on tyrosine. Ca^{2+} increases result in dephosphorylation of NFATc4 and translocation of NFAT to the nucleus where it regulates target genes.

Endothelial dysfunction is a hallmark of aneurysm. Aneurysm is one of the most common manifestations in ADPKD. Also, it has been reported that dysregulation of TRPC4 results in vascular endothelial dysfunction. Inhibition of PC1-mediated TRPC4β activity induces endothelial dysfunction, as evidenced by the reduction of cells migration and disruption of cell-cell junctions. Based on these findings, I propose activation of PC1-mediated TRPC4β in endothelial cells (**Figure 38**). In conclusion, the main finding of this study are as following: (1) PC1 (FL) but no PC1 (CTF) activates TRPC4β by $G\alpha_{i3}$. (2) PC1 and TRPC4β increases Ca^{2+}-dependent STATs and NFAT activation. (3) PC1-mediated TRPC4β activity is required for endothelial cells migration and junctions formation.

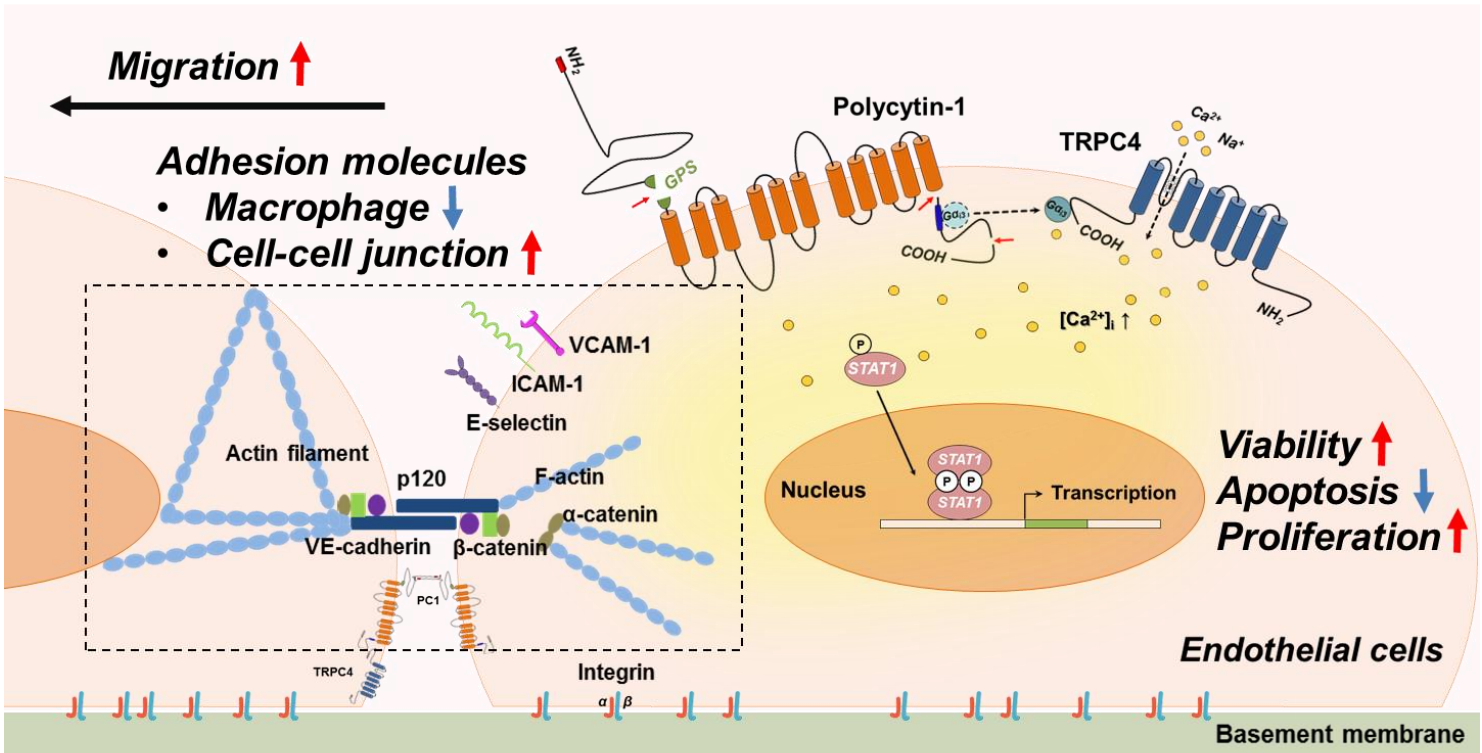

Figure 38. Schematic summary of the proposed model.

REFERENCES

1. Torres VE et al. Autosomal dominant polycystic kidney disease. Lancet. 2007 Apr 14;369(9569):1287-301.
2. Lanoix J et al. Dysregulation of cellular proliferation and apoptosis mediates human autosomal dominant polycystic kidney disease (ADPKD). Oncogene. 1996 Sep 19;13(6):1153-60.
3. Kim H et al. Depletion of PKD1 by an antisense oligodeoxynucleotide induces premature G1/S-phase transition. Eur J Hum Genet. 2004 Jun;12(6):433-40.
4. Li X et al. Polycystin-1 and polycystin-2 regulate the cell cycle through the helix-loop-helix inhibitor Id2. Nat Cell Biol. 2005 Dec;7(12):1202-12. Epub 2005 Nov 27.
5. Manzati E et al. The cytoplasmic C-terminus of polycystin-1 increases cell proliferation in kidney epithelial cells through serum-activated and Ca(2+)-dependent pathway(s). Exp Cell Res. 2005 Apr 1;304(2):391-406. Epub 2004 Dec 15.

6. Nickel C et al. The polycystin-1 C-terminal fragment triggers branching morphogenesis and migration of tubular kidney epithelial cells. J Clin Invest. 2002 Feb;109(4):481-9.
7. Polgar K et al. Disruption of polycystin-1 function interferes with branching morphogenesis of the ureteric bud in developing mouse kidneys. Dev Biol. 2005 Oct 1;286(1):16-30.
8. Aguiari G et al. K562 erythroid and HL60 macrophage differentiation downregulates polycystin, a large membrane-associated protein. Exp Cell Res. 1998 Oct 10;244(1):259-67.
9. Boca M et al. Polycystin-1 induces resistance to apoptosis through the phosphatidylinositol 3-kinase/Akt signaling pathway. J Am Soc Nephrol. 2006 Mar;17(3):637-47. Epub 2006 Feb 1.
10. Bhunia AK et al. PKD1 induces p21waf1 and regulation of the cell cycle via direct activation of the JAK-STAT signaling pathway in a process requiring PKD2. Cell. 2002 Apr 19;109(2):157-68.

11. Vandorpe DH et al. The cytoplasmic C-terminal fragment of polycystin-1 regulates a Ca2+-permeable cation channel. J Biol Chem. 2001 Feb 9;276(6):4093-101. Epub 2000 Oct 23.
12. Babich V et al. The N-terminal extracellular domain is required for polycystin-1-dependent channel activity. J Biol Chem. 2004 Jun 11;279(24):25582-9. Epub 2004 Apr 1.
13. Pelucchi B et al. Nonspecific cation current associated with native polycystin-2 in HEK-293 cells. J Am Soc Nephrol. 2006 Feb;17(2):388-97. Epub 2006 Jan 5.
14. Parnell SC et al. The polycystic kidney disease-1 protein, polycystin-1, binds and activates heterotrimeric G-proteins in vitro. Biochem Biophys Res Commun. 1998 Oct 20;251(2):625-31.
15. Delmas P et al. Constitutive activation of G-proteins by polycystin-1 is antagonized by polycystin-2. J Biol Chem. 2002 Mar 29;277(13):11276-83. Epub 2002 Jan 10.
16. Hughes J et al. The polycystic kidney disease 1 (PKD1) gene encodes a novel protein with multiple cell

recognition domains. Nat Genet. 1995 Jun;10(2):151-60.

17. Qian F et al. Cleavage of polycystin-1 requires the receptor for egg jelly domain and is disrupted by human autosomal-dominant polycystic kidney disease 1-associated mutations. Proc Natl Acad Sci U S A. 2002 Dec 24;99(26):16981-6. Epub 2002 Dec 13.
18. Lakkis M and Zhou J. Molecular complexes formed with polycystins. Nephron Exp Nephrol. 2003 Jan;93(1):e3-8.
19. Hanaoka K et al. Co-assembly of polycystin-1 and -2 produces unique cation-permeable currents. Nature. 2000 Dec 21-28;408(6815):990-4.
20. Merrick D et al. Polycystin-1 cleavage and the regulation of transcriptional pathways. Pediatr Nephrol. 2014 Apr;29(4):505-11. doi: 10.1007/s00467-013-2548-y. Epub 2013 Jul 4.
21. Low SH et al. Polycystin-1, STAT6, and P100 function in a pathway that transduces ciliary mechanosensation and is activated in polycystic kidney disease. Dev Cell. 2006 Jan;10(1):57-69.

22. Kim E et al. The polycystic kidney disease 1 gene product modulates Wnt signaling. J Biol Chem. 1999 Feb 19;274(8):4947-53.

23. Shillingford JM et al. The mTOR pathway is regulated by polycystin-1, and its inhibition reverses renal cystogenesis in polycystic kidney disease. Proc Natl Acad Sci U S A. 2006 Apr 4;103(14):5466-71. Epub 2006 Mar 27.

24. Puri S et al. Polycystin-1 activates the calcineurin/NFAT (nuclear factor of activated T-cells) signaling pathway. J Biol Chem. 2004 Dec 31;279(53):55455-64. Epub 2004 Oct 5.

25. Li Y et al. Polycystin-1 interacts with inositol 1,4,5-trisphosphate receptor to modulate intracellular Ca2+ signaling with implications for polycystic kidney disease. J Biol Chem. 2009 Dec 25;284(52):36431-41. doi: 10.1074/jbc.M109.068916. Epub 2009 Oct 23.

26. Calò V et al. STAT proteins: from normal control of cellular events to tumorigenesis. J Cell Physiol. 2003 Nov;197(2):157-68.

27. Low SH et al. Polycystin-1, STAT6, and P100 function in a pathway that transduces ciliary mechanosensation and is activated in polycystic kidney disease. Dev Cell. 2006 Jan;10(1):57-69.
28. Rao A et al. Transcription factors of the NFAT family: regulation and function. Annu Rev Immunol. 1997;15:707-47.
29. Nilius B et al. Transient receptor potential cation channels in disease. Physiol Rev. 2007 Jan;87(1):165-217.
30. Hofherr A and Köttgen M. TRPP channels and polycystins. Adv Exp Med Biol. 2011;704:287-313. doi: 10.1007/978-94-007-0265-3_16.
31. Lewby LJ et al. Identification, characterization, and localization of a novel kidney polycystin-1-polycystin-2 complex. J Biol Chem. 2002 Jun 7;277(23):20763-73. Epub 2002 Mar 18.
32. Schaefer M et al. Receptor-mediated regulation of the nonselective cation channels TRPC4 and TRPC5. J Biol Chem. 2000 Jun 9;275(23):17517-26.

33. Jeon JP et al. Selective Gαi subunits as novel direct activators of transient receptor potential canonical (TRPC)4 and TRPC5 channels. J Biol Chem. 2012 May 18;287(21):17029-39. doi: 10.1074/jbc.M111.326553. Epub 2012 Mar 28.
34. Graziani A et al. Cell-cell contact formation governs Ca2+ signaling by TRPC4 in the vascular endothelium: evidence for a regulatory TRPC4-beta-catenin interaction. J Biol Chem. 2010 Feb 5;285(6):4213-23. doi: 10.1074/jbc.M109.060301. Epub 2009 Dec 8.
35. Mariani L et al. Cerebral aneurysms in patients with autosomal dominant polycystic kidney disease--to screen, to clip, to coil? Nephrol Dial Transplant. 1999 Oct;14(10):2319-22.
36. Xu HW et al. Screening for intracranial aneurysm in 355 patients with autosomal-dominant polycystic kidney disease. Stroke. 2011 Jan;42(1):204-6. doi: 10.1161/STROKEAHA.110.578740. Epub 2010 Dec 16.
37. Pirson Y et al. Management of cerebral aneurysms in autosomal dominant polycystic kidney disease. J Am Soc Nephrol. 2002 Jan;13(1):269-76. 38.

38. Trudel M et al. The Role of G-Protein-Coupled Receptor Proteolysis Site Cleavage of Polycystin-1 in Renal Physiology and Polycystic Kidney Disease. Cells. 2016 Jan 21;5(1). pii: E3. doi: 10.3390/cells5010003.
39. O Bukanov N et al. Functional polycystin-1 expression is developmentally regulated during epithelial morphogenesis in vitro: downregulation and loss of membrane localization during cystogenesis. Hum Mol Genet. 2002 Apr 15;11(8):923-36.
40. Ecder T and Schrier RW. Cardiovascular abnormalities in autosomal-dominant polycystic kidney disease. Nat Rev Nephrol. 2009 Apr;5(4):221-8. doi: 10.1038/nrneph.2009.13.
41. Wei W et al. Characterization of cis-autoproteolysis of polycystin-1, the product of human polycystic kidney disease 1 gene. J Biol Chem. 2007 Jul 27;282(30):21729-37. Epub 2007 May 24.
42. Chauvet V et al. Mechanical stimuli induce cleavage and nuclear translocation of the polycystin-1 C terminus. J Clin Invest. 2004 Nov;114(10):1433-43.

43. Chapin HC et al. Polycystin-1 surface localization is stimulated by polycystin-2 and cleavage at the G protein-coupled receptor proteolytic site. Mol Biol Cell. 2010 Dec;21(24):4338-48. doi: 10.1091/mbc.E10-05-0407. Epub 2010 Oct 27.

44. Merrick D et al. The γ-secretase cleavage product of polycystin-1 regulates TCF and CHOP-mediated transcriptional activation through a p300-dependent mechanism. Dev Cell. 2012 Jan 17;22(1):197-210. doi: 10.1016/j.devcel.2011.10.028. Epub 2011 Dec 15.

45. Xu Q et al. Structural insights into the mechanism of intramolecular proteolysis. Cell. 1999 Sep 3;98(5):651-61.

46. Schaefer M et al. Receptor-mediated regulation of the nonselective cation channels TRPC4 and TRPC5. J Biol Chem. 2000 Jun 9;275(23):17517-26.

47. Kang TM et al. The properties of carbachol-activated nonselective cation channels at the single channel level in guinea pig gastric myocytes. Jpn J Pharmacol. 2001 Mar;85(3):291-8.

48. Kim S et al. The polycystin complex mediates Wnt/Ca(2+) signalling. Nat Cell Biol. 2016 Jul;18(7):752-64. doi: 10.1038/ncb3363. Epub 2016 May 23.
49. Talbot JJ et al. Polycysitn-1 regulates STAT activity by a dual mechanism. Proc Natl Acad Sci U S A. 2011 May 10;108(19):7985-90. doi: 10.1073/pnas.1103816108. Epub 2011 Apr 25.
50. Levy DE and Darnell JE Jr Stats: transcriptional control and biological impact. Nat Rev Mol Cell Biol. 2002 Sep;3(9):651-62.
51. Somlo S, Ehrlich B. Human disease: calcium signaling in polycystic kidney disease. Curr Biol. 2001 May 1;11(9):R356-60.
52. Berridge MJ. Calcium signalling and cell proliferation. Bioessays. 1995 Jun;17(6):491-500.
53. Hardingham GE et al. Distinct functions of nuclear and cytoplasmic calcium in the control of gene expression. Nature. 1997 Jan 16;385(6613):260-5.

54. Rao A et al. Transcription factors of the NFAT family: regulation and function. Annu Rev Immunol. 1997;15:707-47.

55. Earley S and Brayden JE. Transient receptor potential channels and vascular function. Clin Sci (Lond). 2010 Apr 7;119(1):19-36. doi: 10.1042/CS20090641.

56. Inoue R et al. Pathophysiological implications of transient receptor potential channels in vascular function. Curr Opin Nephrol Hypertens. 2008 Mar;17(2):193-8. doi: 10.1097/MNH.0b013e3282f52467.

57. Yao X and Garland CJ. Recent developments in vascular endothelial cell transient receptor potential channels. Circ Res. 2005 Oct 28;97(9):853-63.

58. Boulter C et al. Cardiovascular, skeletal, and renal defects in mice with a targeted disruption of the Pkd1 gene. Proc Natl Acad Sci U S A. 2001 Oct 9;98(21):12174-9. Epub 2001 Oct 2.

59. Kim K et al. Polycystin 1 is required for the structural integrity of blood vessels. Proc Natl Acad Sci U S A. 2000 Feb 15;97(4):1731-6.

60. Krasnoperov VG et al. alpha-Latrotoxin stimulates exocytosis by the interaction with a neuronal G-protein-coupled receptor. Neuron. 1997 Jun;18(6):925-37.

61. Paavola KJ et al. The N terminus of the adhesion G protein-coupled receptor GPR56 controls receptor signaling activity. J Biol Chem. 2011 Aug 19;286(33):28914-21. doi: 10.1074/jbc.M111.247973. Epub 2011 Jun 27.

62. Rossetti S et al. Association of mutation position in polycystic kidney disease 1 (PKD1) gene and development of a vascular phenotype. Lancet. 2003 Jun 28;361(9376):2196-201.

63. Murcia NS et al. New insights into the molecular pathophysiology of polycystic kidney disease. Kidney Int. 1999 Apr;55(4):1187-97.

64. Lanoix J et al. Dysregulation of cellular proliferation and apoptosis mediates human autosomal dominant polycystic kidney disease (ADPKD). Oncogene. 1996 Sep 19;13(6):1153-60.

65. Chalouhi N et al. Review of cerebral aneurysm formation, growth, and rupture. Stroke. 2013 Dec;44(12):3613-22. doi: 10.1161/STROKEAHA.113.002390. Epub 2013 Oct 15.

국문 초록

다낭신은 흔한 유전질환으로 폴리시스틴-1 (polycystin-1)과 폴리시스틴-2 (polycystin-2) 돌연변이에 의해 발생한다. 다낭신 환자에서 고혈압과 동맥류가 흔히 동반되는데 이는 내피세포의 기능이상과 밀접한 관련이 있다. 폴리시스틴-1은 비전형적인 G 단백 연결 수용체로 자가 절단에 의하여 G 단백이 활성화되고, 활성화된 G 단백을 매개로 세포 내 신호 전달을 유도하며, 또한 이온통로 활성화에 의한 세포반응이 보고된 바 있다. TRPC4는 칼슘 투과성을 갖는 양이온 통로이며 G 단백의 특정 아형 ($G\alpha_i$)에 의하여 활성화된다. 본 연구에서는 폴리시스틴-1이 G 단백 연결 수용체로 작용하여 G 단백을 활성화하고 그 결과로 TRPC4 활성을 일으킬 가능성을 가설로 세우고 실험을 진행하여 다음과 같은 결과를 얻었다. 폴리시스틴-1의 C-말단기는 G 단백질 결합 부위를 포함하고 있으며, 억제성 G 아형 단백질 중 $G\alpha_{i3}$ 와 선택적으로 결합하였다. 폴리시스틴-1에 의한 TRPC4 활성 증가는 $G\alpha_{i3}$를 매개로 해서 이루어지는데, 그 기전으로는 폴리시스틴-1이 절단되면서 C-말단기에 결합된 $G\alpha_{i3}$가 유리되는 것이 중요한 과정이었다. TRPC4로 유입된 칼슘은 signal transducer and activator of transcription (STATs)와 nuclear factor of activated T-cells (NFAT) 전사인자를 활성시켜서 세포증식과 사멸을 조절하였다. 내피세포에서 폴리시스틴-1과 TRPC4의 내인성 발현 및 칼슘유입을 확인하였으며, 이들의 발현을 억제하거나 약리학적 차단제를 투여하면 내피 세포의 이동이 저해되고 내피 접합이 약화되었다. 이상의 결과는 폴리시스틴-1에 의한 TRPC4 활성이 내피세포 단일층 형성 및 내피세포를 통한 물질

들의 투과도에 중요하며, 다낭신에 동반되어 나타나는 동맥류 발생기전 및 치료에서 TRPC4가 표적임을 시사한다.

주요어 : 상염색제 우성 다낭성 신종, 폴리시스틴-1, G 단백질 연결 수용체, 비선택성 양이온통로, 칼슘, 전사인자, T 세포활성화인자, 혈관내피세포

학 번 : 2013-23520